To be submitted to The Astrophysical Journal, May 2002

Is a minor-merger driving the nuclear activity in the Seyfert 2 galaxy NGC 2110?

Rosa M. González Delgado

Instituto de Astrofísica de Andalucía (CSIC), Apdo. 3004, 18080 Granada, Spain

Electronic mail: rosa@iaa.es

Santiago Arribas

Space Telescope Science Institute, 3700 San Martin Drive, Baltimore, MD 21218

Electronic mail: arribas@stsci.edu

Enrique Pérez

Instituto de Astrofísica de Andalucía (CSIC), Apdo. 3004, 18080 Granada, Spain

Electronic mail: eperez@iaa.es

and

Timothy Heckman

Department of Physics & Astronomy, JHU, Baltimore, MD 21218

Adjunct Astronomer at STScI

Electronic mail: heckman@pha.jhu.edu

ABSTRACT

We report on a detailed morphological and kinematic study of the isolated non-barred nearby Seyfert 2 galaxy NGC 2110. We combine Integral Field optical spectroscopy, with long-slit and WFPC2 imaging available in the HST archive to investigate the fueling mechanism in this galaxy. Previous work (Wilson & Baldwin 1985) concluded that the kinematic center of the galaxy is displaced $\sim$ 220 pc from the apparent mass center of the galaxy, and the ionized gas follows a remarkably normal rotation curve. Our analysis based on the stellar kinematics, 2D ionized gas velocity field and dispersion velocity, and high spatial resolution morphology at V, I and Hα reveals that: 1) The kinematic center of NGC 2110 is at the nucleus of the galaxy. 2) The ionized gas is not in pure rotational motion. 3) The morphology of the 2D distribution of the emission line widths suggests the presence of a minor axis galactic outflow. 4) The nucleus is blue-shifted with respect to the stellar systemic velocity, suggesting the NLR gas is out-flowing due to the interaction with the radio jet. 5) The ionized gas is red-shifted $\sim$ 100 km/s over the corresponding rotational motion south of the nucleus, and 240 km/s with respect to the nuclear stellar systemic velocity. This velocity is coincident with the HI red-shifted absorption velocity detected by Gallimore et al (1999). We discuss the possibility that the kinematics of the south ionized gas could be perturbed by the collision with a small satellite that impacted on NGC 2110 close to the center with a highly inclined orbit. Additional support for this interpretation are the radial dust lanes and tidal debris detected in the V un-sharp masked image. We suggest that a minor-merger may have driven the nuclear activity in NGC 2110.

Subject headings: galaxies: active – galaxies: nuclei – galaxies: Seyfert – galaxies: individual (NGC 2110) galaxies: kinematics and dynamics

1. Introduction

The two most important questions concerning active galactic nuclei (AGN) are the fundamental nature of their energy source and the mechanism by which the nuclear activity is fueled. Even though it is widely accepted that the energy source originates in the accretion of mass onto a central super-massive black hole (SMBH), starbursts could also play an important role in the same galaxies (e.g. González Delgado 2001; Veilleux 2001, and references therein). In fact, many examples have been reported in which the two phenomena co-exist together. At the high-luminosity regime, ULIRGs are the best examples (Lutz & Tacconi 1999). Powerful starbursts are also found in the central $\sim$ 100 pc of less luminous AGN, such as Seyfert 2 galaxies (Heckman et al 1997; González Delgado et al 1998), and even at smaller spatial scales ($\sim$ few pc), as it is the case of the low luminosity AGN NGC 4303 (Colina et al 2002).

The origin of the gas that fuels the central engine and the mechanism that brings the gas to the very central region are still controversial. Observations of high luminosity AGNs indicate that QSOs and ULIRGs have been gas-rich mergers (Sanders et al 1988; Canalizo & Stockton 2001). However, in low luminosity AGNs, the fueling mechanism remains unclear.

Early investigations in Seyfert galaxies have also suggested that galaxy-interaction could provide the gas fueling onto the SMBH (e.g. Noguchi 1988; Mihos & Hernquist 1996). Early research suggested that there is an excess of companions in Seyfert galaxies (Dahari 1984). However, this result has not been confirmed more recently (De Robertis, Yee & Hayhoe 1998; Rafanelli et al 1995). Thus, the galaxy-interaction hypothesis can be ruled out as the main fueling mechanism in Seyfert galaxies.

The non-axisymmetric gravitational potential originated by a large scale bar in the host galaxy has also been suggested as an efficient way to drive the gas to the central region (Shlosman, Begelman & Frank 1990; Athanassoula 1992). However, it can be ruled out as a general mechanism because an excess of bars in Seyfert galaxies has not been confirmed observationally (Adams 1977; Moles, Márquez & Pérez 1995; Hunt et al 1997; Maiolino, Risaliti & Salvati 1998). Studies based on near-infrared imaging, known to trace the stellar bars better than the optical observations, arrive also at contradictory results. Based on HST (NICMOS) observations Mulchaey & Regan (1997), Regan & Mulchaey (1999) and Martini & Pogge (1999) find no evidence for an excess of stellar bars in Seyferts. On the opposite, Knapen, Shlosman, & Peletier (2000) found an excess in the sample of CfA Seyfert galaxies with respect to a control sample. However, this excess of bars in CfA Seyfert galaxies disappears when galaxies that are in interaction are excluded from the statistics (Márquez et al 2000).

Minor merger between a disk galaxy and a nucleated less massive galaxy is also proposed as an alternative fueling mechanism (García-Lorenzo et al 1997; de Robertis et al 1998; Taniguchi 1999). In this context, it is interesting to note that some kinematic peculiarities found in NGC 1068 have been interpreted by García-Lorenzo et al (1997 and 1999) as the result of a minor merger event. Since most galaxies have satellites (Zaritsky et al 1997), it is likely that minor mergers drive the fueling mechanism for most of the isolated Seyfert galaxies. However, there is not yet observational proof of this scenario.

NGC 2110 is a nearby ($\sim$ 31 Mpc), early type S0, isolated galaxy, showing a Seyfert 2 nucleus (McClintok et al. 1979; Shuder 1980). This galaxy has been extensively studied at radio, NIR, optical, UV and X-ray wavelengths. These studies have revealed a number of interesting properties in this object, making it a good target to investigate the minor-merger hypothesis as the mechanism that drives the gas to the center and feeds the AGN in NGC 2110. Its main properties can be summarized as follow:

- It is classified as a narrow-line X-ray galaxy (Bradt et al 1978) due to the strong X-ray emission, having a hard X-ray luminosity (2-10 KeV) comparable to those of Seyfert 1 galaxies (Weaver et al 1995). Soft X-ray emission is also detected at 4 arcsec North of the nucleus (Weaver et al 1995).

- VLA radio continuum maps reveal a symmetrical jet-like radio emission extended 4 arcsec along the North-South direction (Ulvestad & Wilson 1983; Nagar et al 1999). More recent VLBA observations at 3.6 cm also show a compact (≤ 1 pc) radio core aligned with the 400 pc scale radio jet (Mundell et al 2000).

- Ground-based narrow band ([OIII] and Hα+[NII]) images reveal extended emission up to 10 arcsec showing an S-shape morphology in the North-South direction (Wilson, Baldwin and Ulvestad 1985; Pogge 1989). HST pre-Costar [OIII] and Hα+[NII] images confirm the alignment of the optical and radio jet, but only a loose anti-correlation between the brightest optical and radio knots was found (Mulchaey et al 1994). Ferruit et al (1999) have obtained HST+FOC UV, and optical spectra of the jet to investigate the mechanism that ionizes the extended gas. They suggest that the ionized high excitation gas is produced by photoionization by fast-shock waves probably generated by the propagation of the radio ejecta into the ISM of the host galaxy. Shocks, driven by the radio jet, could be also responsible for the strong [FeII] λ1.2567 μm nebular emission detected in its nuclear and circumnuclear region (Storchi-Bergmann et al 1999; Knop et al 2001).

- From the morphological point of view, the optical continuum (Malkan et al 1998) and NICMOS/WFPC color maps (Quillen et al 1999) show clear asymmetries in the central region. Dust lanes at 1 and 4 arcsec to the west of the nucleus are detected.

- The nuclear stellar population was studied by González Delgado, Heckman, & Leitherer (2001) to look for signatures of starbursts. Its optical continuum (stellar features and spectral energy distribution) is well explained by an old stellar population with a small contribution from a power-law. Thus, no obvious signs of a young (age ≤ 1 Gyr) stellar population were found.

- The kinematics of the circumnuclear ionized gas region was studied by Wilson and Baldwin (1985) and Wilson et al (1985). They reported a rotation pattern remarkably similar to that expected for spiral galaxies. They also found that the rotation center was not coincident with the optical (and radio) nucleus, but was located 1.7 arcsec (220 pc) to the south of the nucleus. They also reported the presence of asymmetric profiles in the [OIII] nebular lines, south and east of the nucleus.

- HI absorption has been detected in NGC 2110 by Gallimore et al (1999) located south of the maximum of the radio continuum source. This absorption has a velocity of 2626 km/s; red-shifted by about 290 km/s with respect to the systemic velocity, 2335 km/s, calculated by Strauss et al (1992) using the nuclear optical emission lines.

Here, we present new Integral Field Spectroscopic (IFS) data at optical wavelengths of the circumnuclear region of NGC 2110. This technique is ideal for studying an asymmetric and complex object like NGC 2110 since it provides 2D spectral information of relevant spectral features (i.e., velocity fields, velocity dispersion maps, line intensity maps, continuum maps, etc) simultaneously and, therefore, without the uncertainties associated with centering, reference systems, etc. In addition to these IFS data, we also present new longslit spectroscopy to study the stellar kinematics. These data, together with some WFPC2 images retrieved from the HST archive, allow us to investigate the kinematic peculiarities found in NGC 2110 and their possible connection with the fueling mechanism of the AGN in NGC 2110. The paper is organized as follows: In Section 2 we present the observations and data reduction. Section 3 presents the analysis of the stellar and ionized gas distribution, and section 4 the gas and stellar kinematics. We discuss our results and their implications in section 5. The conclusions and summary are in section 6.

2. Observations and data reduction

Two types of observations have been carried out: 1) Integral field spectroscopy and 2) long-slit spectroscopy. In addition, HST WFPC2 images have been retrieved from the ST-ECF archive.

2.1. Integral field spectroscopy

NGC 2110 was observed with the INTEGRAL system (Arribas et al 1998) and the Wide Field Fiber Optic Spectrograph (Bingham et al 1994) attached to the 4.2m William Herschel Telescope at the Roque de los Muchachos Observatory during 1999 February 10. We used the SB2 bundle of fibers, consisting of 219 fibers with a core diameter of 0.9 arcsec each. The 189 data fibers are arranged forming a rectangle with a 16.5×12.3 arcsec field of view. A ring of 30 fibers, at 45 arcsec from the center, is intended for collecting the background light. We observed with the R600B grating, covering the 3700–7000 Å spectral range with a linear dispersion of 3 Å/pixel. The mean effective spectral resolution is 5.3 Å. The total integration time was 7200 s split into four 1800 s exposures. The airmass of the object during the observations was between 1.25 and 1.45, and the seeing $\sim$ 1.0-1.2 arcsec.

The reduction of the spectra was performed with the IRAF[1] data processing software.

[1]IRAF is distributed by the National Optical Astronomy Observatories, which are operated by the As-

We followed the standard procedures applied to spectra obtained with two-dimensional fiber spectrographs (Arribas et al 1997). They consist of: 1) Bias subtraction. 2) Cosmic rays rejection. 3) Definition and extraction of the 219 apertures. 4) Arc lines identification and dispersion correction. 5) Flat-field and throughput correction. 6) Sky subtraction. 7) Atmospheric extinction correction and flux calibration. The typical wavelength calibration error 0.2-0.3 Å, gives velocity uncertainties of 10-15 km/s.

To do the flux calibration, we have also observed with the bundle SB2 the spectroscopic standard Feige 34. Two 180 s exposures were taken; one of them was taken through a color filter that blocks the second-order blue light from wavelengths below 4950 Å. The sensitivity function was built using the stellar spectrum of one of the fibers, then scaling it by a factor that represents the fraction of the flux detected by this fiber with respect to the total flux.

2.2. Analysis of the Integral field data

Two-dimensional maps of some spectral features, such as continuum, absorption lines equivalent width, line emission fluxes, and radial and dispersion velocity were obtained from the fibers individual spectra with a program that uses a Renka+Cline two-dimensional interpolation method. This routine (NAG-E01SAF) transforms a file with the actual position of the fibers in the focal plane of the telescope and the spectral feature into a regularly spaced image, and it guarantees that the constructed surface is continuous and has continuos first derivatives. The interpolant is then evaluated regularly each 0.0846 arcsec on a grid of 201 $\times$ 201 pixels to create the maps. Note that the continuity conditions imposed to the interpolant allows one to evaluate it with a fine sampling. Although this procedure does not modify the effective spatial resolution, it improves the general appearance of the maps.

Prior to interpolation, the kinematical and line intensity information for each fiber was obtained measuring the main nebular lines such as Hβ, [OIII] λ5007, [OI] λ6300, Hα, [NII] λ6584, and [SII] λ6717, 6731. The measurements were done by fitting gaussians to the nebular lines using the program *Longslit* (Wilkins & Axon 1991). These fits determine the central wavelength, the emission line width, the flux and the continuum. Alternatively, the continuum and emission line images were also obtained integrating the fluxes between appropriate wavelength ranges. These images reveal the same continuum and nebular emission structures that those obtained by fitting gaussians to the nebular lines. The image obtained as the difference between the map obtained through the gaussian fitting procedure and that obtained

---

sociation of Universitites for Research in Astronomy, Inc., under cooperative agreement with the National Science Foundation

integrating the fluxes does not show any significant residual emission structure. Thus, this result indicates, that the gaussian fitting method works well to provide the continuum and emission line structures of NGC 2110.

2.3. Long-slit spectroscopy

NGC 2110 was observed using the Richey-Chretien spectrograph attached to 4m Mayall Telescope at the KPNO during 1996 February 15 and 16. The detector was a T2KB CCD chip with a spatial sampling of 0.7 arcsec/pixel. The slit width was set to 1.5 arcsec and it was oriented near the paralactic angle, P.A= 6°. We used the gratings BL420 and KPC-007 to cover the spectral range, 6600-9100 Å, and 3400-5500 Å, respectively. The linear dispersion is 1.52 Å/pixel for the red and 1.39 Å/pixel for blue spectral range. The effective spectral resolution is $\sim$3 Å. One exposure of 1800 s was taken at the red, and 2 exposures of 900 s each at the blue wavelengths. The seeing was about 1.5 arcsec.

Data reduction was performed using the FIGARO[2] data processing software. We followed the standard procedures applied to long-slit spectra: 1) Bias and flat-field correction. 2) Two-dimensional wavelength calibration using ARC2D (Wilkins & Axon 1991). 3) Atmospheric extinction correction and flux calibration. Several spectroscopic standards were observed with a 10 arcsec wide slit during the night. In addition, several velocity template K giant stars were observed for the kinematic analysis.

2.4. HST archival data

We obtained three sets of WFPC2 images of NGC 2110 from the ST-ECF HST archive. The images were taken through three different filters: F606W, F919W and FR680P15. The filter F606W (λ=6010.6 Å, $\delta\lambda$=1497 Å) (P.I. Malkan) includes emission from the strong lines [OIII] λ5007 and Hα. The integration time was 500s. The filter F791W (λ=8006 Å, $\delta\lambda$=1304 Å) (P.I. Mundell) transmits mainly the red continuum of the object, and it is free of contamination from strong emission lines; we refer to it as I image. The integration consisted of 2 $\times$ 120s exposures. FR680P15 (P.I. Mundell) is a linear ramp filter designed to observe the emission line Hα. The band is centered at 6610 Å, and it has a width of 41 Å; this filter also includes the emission line [NII] λ6548. The unvigneted field of view through this filter is about 9 arcsec. The total integration time of 1200 s was splitted into four exposures.

[2]Software from the Starlink Project funded by the UK PPARC

We refer to it as Hα. The three sets of observations place the nucleus of NGC 2110 in the PC. The central part of NGC 2110 (corresponding to most of the emission detected in the galaxy) is thus sampled at 0.046 arcsec/pixel.

We use the standard pipeline reduction procedures. The individual frames of the I and Hα images were combined with *crreject* command to eliminate the cosmic rays. To produce a continuum free Hα image, the I image was scaled down by a factor of 3 and subtracted from the Hα plus underlying continuum. The scaling of the I image was performed by visual inspection through photometric cuts along the major and minor axes. This method was preferred to the direct scaling of the filter widths, because as seen in the spectra (see Figure 2) the continuum is quite red, thus, there is a strong color component in the scaling from I to the Hα wavelength band, that is position dependent.

3. Stellar and ionized gas distribution

Figure 1 shows the individual calibrated spectra corresponding to the 189 fibers in the spectral ranges which include Hβ and [OIII] λ4959, 5007 (a) and Hα and [NII] λ6548, 6584 (b). Figure 2 shows the nuclear spectrum from the fiber 110 corresponding to the maximum of the continuum and presumably the AGN, and two circumnuclear spectra corresponding to fiber 123 ($\sim$ 3 arcsec north from the nucleus) and fiber 110 ($\sim$ 2 arcsec south from the nucleus). These two spectra have been chosen to show the north-south asymmetry in the excitation, measured as the [OIII]/Hβ ratio. In addition to the nebular lines, the spectra show prominent stellar absorption lines, such as CaII K, G band and Mgb.

3.1. Continuum morphology

Figure 3a shows in grey scale the I image of NGC 2110 in the PC. Out of the central 2 arcsec, the red continuum distribution is very smooth and typical of an early type galaxy, with the isophotes oriented along P.A=160-170°. A mosaic image built combining the PC and the three WF cameras do not show any additional information about low surface brightness continuum in the out-skirt of the galaxy, that could reflect any distortion of the morphology. However, in the circumnuclear region, NGC 2110 shows an asymmetry of its inner isophotes in the east-west direction due to the dust lanes that run north-south between 1 and 2 arcsec west of the nucleus, and trace a clear spiral patern around the nucleus. These dust lane structures are shown more clearly in the un-sharp masked I image (Figure 3b). Nuclear spiral dust lanes are commonly found in HST observations of active galaxies (Regan &

Mulchaey 1999; Martini & Pogge 1999; Pogge & Martini 2002). They would correspond to spiral arms formed in non-self-gravitating disk by hydrodynamic instabilities, and they could represent the paths of the gas infalling to the center of the galaxy. This image has been obtained by dividing the original I image by a 31 pixel median filtered version of the same image. However, the same structures are seen if the original I image is divided by the model obtained fitting ellipses to the continuum distribution (see below).

To constrain the photometric center, the position angle of the photometric major axis, and the inclination of the disk of NGC 2110 we have performed an isophotal fit to the I image using the iraf task *ellipse* on the *stsdas* analysis package. No constraints were imposed on the fits, thus, the resulting ellipses are all free in the different parameters (center, ellipticity, etc). The fitted ellipses are shown over the grey scale I image (Figure 3a). The major axis of the fitted ellipses define the position angle of the photometric major axis position angle. This position angle is 163.5° from North to East. The inclination of the disk, obtained from the ellipticity of the isophotes, is 42°. Both values are in very good agreement with previously published values (Wilson & Baldwin 1985). To get the photometric center, we have calculated the difference between the center of each fitted ellipse and the location of the maximum of the I image. The median residuals are 0.13 arcsec in RA and 0.07 arcsec in Dec. The largest difference come from the isophotes more affected by the dust lanes; while the outer isophotes give smaller residuals. Therefore, the isophotes indicate that the photometric center of the galaxy is indeed at the maximum of the I band flux.

Figure 4a presents the central emission through the filter F606W. It shows clearly the east-west asymmetry at 1-2 arcsec west of the nucleus due to the dust lanes. The inner 2 arcsec isophotes show a steeper gradient to the west. We have convolved this image with a gaussian (Figure 4b) to compare it visually with the IFS continuum images. Figure 4c shows the continuum obtained from the observed IFS spectra after integrating the fluxes between 5320 and 5440 Å.

3.2. Ionized gas morphology

The HST Hα continuum-free image is plotted in Figure 5a. It shows a nuclear point source plus the circumnuclear emission extended along the north-south direction. It has a bright plume extended 1 arcsec from the nucleus to the north that is aligned with the radio jet. This plume is narrowest toward the nucleus. At 1 arcsec south, there are two Hα clouds that may be related with the southern radio lobe. However, as it has been previously reported by Mulchaey et al (1994), the Hα brightness distribution of the plume and the two clouds appear to be anti-correlated with the maximum of the lobes of the radio jet. At larger scales, the Hα emission shows an S-shaped distribution that extends 5 arcsec to the north and 4 arcsec to the south. The north-side of the S-shaped ionized gas morphology follows the inner edge of the dust lanes distribution seen in the un-sharp masked I Image (Figure 6). However, at the south, the ionized gas is in between the two dust lanes, but it does not follow so well the curve of the dust lane. Therefore, this large-scale ionized gas distribution could be reflecting the gas flows towards the nucleus that is photoionized by the AGN.

The emission line maps of Hβ, [OIII] λ5007, [OI]λ6300, Hα, [NII] λ6584 and [SII] λ6717, 6732 have been also obtained fitting a single gaussian profile to the corresponding nebular line in the IFS. Figure 5 compares the HST Hα image convolved with a gaussian with σ equal to the mean seeing with the IFS Hα and Hβ. The extension of the emission, and the morphology of the large-scale distribution are remarkably equal. However, the inner 1 arcsec gas distribution seen in the HST Hα image is lost in our ground-based observations due to the seeing. Within an uncertainty of 0.2 arcsec, the peak of the optical continuum is coincident with the maximum of the nebular lines.

As previously reported (Wilson et al 1985, Pogge 1989, Mulchaey et al 1994), the [OIII] emission (Figure 7) is more asymmetric than Hα; it is brightest at the north than at the south. The [OIII] emission also extends more than 6 arcsec to the north; however, at the south, it does not show the larger scale S-shape emission detected in the Hα and Hβ emission. This high excitation gas is aligned with the radio jet; however, there is not a one to one correspondence between the optical and the radio jet (Mulchaey et al 1994). The [OI]λ6300, [NII] λ6584 and [SII] λ6717, 6732 images also show an asymmetric morphology, more extended and brighter to the north than to the south. On the north, the emission lines show a similar distribution to Hβ and Hα, but on the south, their morphology is more similar to the [OIII] emission.

Excitation maps have been obtained by dividing the emission line images of [OIII] and [NII] by Hβ and Hα, respectively. These ratios are plotted in Figure 8. There is a clear gradient in the [OIII]/Hβ and [NII]/Hα ratios. Both images show the lowest ratio at the south, between 2 and 4 arcsec from the nucleus. The maximum of the [OIII]/Hβ $\sim$ 10, occurs between 3 and 4 arcsec north of the nucleus. A maximum of the [NII]/Hα, $\sim$ 1.6, occurs near the nucleus.

3.3. Stellar absorption lines

In addition to the nebular lines, the circumnuclear spectra show prominent metallic absorption lines, such as CaII at λ3933 Å, G band at λ4300 Å, and Mgb λ5200 Å. To measure the strength of these absorption features, we have determined for each individual spectrum a pseudo-continuum in selected pivot wavelengths, and we have measured the equivalent widths integrating the fluxes under the pseudo-continuum in defined wavelength windows. We measure the CaII K line in the window 3908-3952 Å, and the G band in the window 4284-4318 Å. The pivot-wavelengths that we use are at 3780, 3810, 3910, 4015, 4140, 4260 and 4430 Å. Once, the equivalent widths are measured, the two-dimensional maps are obtained following the method described in section 2.3.

The spatial distribution of the equivalent widths of the metallic lines in the circumnuclear region allows us to estimate the possible variation of the stellar population as a function of the distance to the nucleus. Thus, relatively low values of the equivalent widths of these lines could be produced by the presence of a young stellar population. Alternatively, values of the equivalent widths lower than those expected by an old population at the nucleus and circumnuclear region can be caused by scattered light from the hidden Seyfert 1 nucleus.

Figure 9 shows the iso-equivalent width contours of the CaII K absorption line. The contours are aligned with the optical jet detected in the emission lines. The strength of this line and of the G band decreases inwards. The minimum value of the CaII equivalent width, $\sim$ 11 Å, occurs nearby the nucleus and at 2 arcsec north, where there is also a maximum of the radio and optical jet. This spatial distribution suggests that extended scattered light from the nucleus could be responsible for the dilution of the strength of the metallic lines. Alternatively, as it has been previously suggested (Cid Fernandes & Terlevich 1995; Cid Fernandes et al 2001) the *featureless continuum* that dilutes the CaII K line from the old stars in the host's bulge could be provided by a very young (few Myr old) stellar population.

4. Ionized gas and stellar kinematics

4.1. Velocity field and velocity dispersion map of the ionized gas

The velocity field was obtained by fitting a single gaussian profile to the emission lines (Hβ, [OIII] λ5007, Hα, [NII] λ6584 and [SII]λ6717, 6731). Although the [OIII] line profile shows evidence for kinematic substructure, the mean velocity field is well represented by the centroid wavelength of the brightest component. In fact, in the central 2 arcsec, a blue weaker component is integrated along the line of sight. This blue component is not clearly detected in Hα, [NII] or [SII] in the IFS data, but kinematic structure is clearly detected in the KPNO data. This is due to a larger excitation of this second component with respect to the main one, combined with the lower spectral resolution of our IFS data.

We have defined the mean nuclear velocity of NGC 2110 as the velocity of the ionized gas in the region where the maximum of the continuum occurs. This velocity estimated from the Hβ and [NII] lines, 2315 km/s (after correcting by the heliocentric velocity of -20 km/s), agrees well with the systemic velocity reported by Strauss et al (1992) and it is 30 km/s larger than the optical line velocity reported in the RC3 (de Vaucouleurs et al 1991). It is also in agreement with the nuclear velocity reported by Wilson et al (1985).

Figure 10 shows the velocity field of the ionized gas as traced by [NII] and [OIII]. These maps clearly show a north-south asymmetry, with a larger velocity gradient in the south than in the north. In fact, over 5 arcsec from the optical nucleus along the major photometric axis, i.e. PA=163°, the velocities change by about +300 km/s towards the south and about -100 km/s towards the north (see also Figure 11). Despite this result, the present velocity field does not support the possibility that the kinematic center of rotation is at 1.7 arcsec towards the south of the optical nucleus. In fact, the iso-velocity lines crossing that point are clearly bent towards the reshifted side of the velocity field and away from the nucleus, far from the expected behaviour for the kinematic minor axis. On the contrary, the iso-velocity lines crossing the optical nucleus, though winding, do not show any preferred side, as expected for the true minor kinematic axis. This clear kinematic asymmetry along the major photometric axis plus the non-uniform distribution of the blue velocity contours, suggest that the circumnuclear gas is not normally rotating ambient, interstellar gas in the disk of the galaxy, as it was previously reported (Wilson et al 1985).

To check the absolute velocity scale and the shape of the velocity field, we have compared the velocity curve obtained from our KPNO data with a cut on the INTEGRAL velocity field along P.A= 6° (Figure 12). We have fitted a gaussian to the KPNO data except in the central 2 arcsec, where two gaussians give a better fit. However, in Figure 12 we have plotted only the velocities of the brightest component. The agreement in amplitude and absolute values between the two curves is very good. Therefore, we are confident about our estimation of the absolute values of the velocity field within uncertainties of 15 km/s.

The velocity dispersion of the gas has been estimated from the FWHM of the gaussian profile fitted to the nebular lines. The INTEGRAL FWHM map has been transformed to a velocity dispersion map after correcting by the instrumental resolution. Due to the variation in focus of the WYFFOS spectrograph as a function of the position on the detector, we have obtained an image with the FWHM of the arc lines spectra measured over the 180 fibers. This image was subtracted quadratically from the FWHM of the emission line images of NGC 2110.

Figure 13 plots the sigma of the INTEGRAL velocity dispersion of the ionized gas traced by [OIII] and [NII] over the photometric isophotes of the continuum at 5000 Å and 6600 Å, respectively. The velocity dispersion shows a bar like morphology oriented along P.A=

60-70°, which is close to the photometric minor axis. The maximum of this sigma velocity dispersion, σ=230 km/s for [NII] and 280-290 km/s for [OIII] (Figure 14), is coincident with the peak of the continuum. This result also suggests that the kinematic center is not shifted 1.7 arcsec to the south of the optical nucleus, but that it is coincident with it. On the other hand, the alignment of the iso-dispersion velocity contours with the minor axis indicates that other non-rotational motions contribute to the kinematics of the circumnuclear ionized gas. Thus, this gas is not in pure rotational motion. This result has been observed in edge-on starbursts (Lehnert & Heckman 1996) and in some Seyferts (Colbert et al 1996). In both cases, the off-nuclear emission line widths are maximal along the galaxy minor axis. It is believed that it is due to a thermal wind driven by the starburst or the AGN.

4.2. Stellar velocity field and velocity dispersion

The stellar velocity curve and the velocity dispersion of NGC 2110 along P.A= 6° has been inferred from the CaII triplet ($\lambda\lambda$ 8498, 8542, 8662) absorption lines via the cross-correlation method (Tonry & Davis 1979). We use the *fxcor* task of IRAF between the NGC 2110 spectra (8500-8800 Å) and two K giant stars that were observed as velocity templates.

The shape of the velocity curve obtained with the two stars is very similar. However, the absolute values are shifted by 40 km/s. This shift is due to the zero velocity of each standard velocity star being different. In fact, the CaII lines are blueshifted with respect to the nominal wavelengths in the spectrum of one of the stars, and red-shifted by a similar amount (about 0.5 Å) in the other star. We take the mean stellar velocity curve. We estimate the systemic velocity as the velocity of the maximum of the continuum at 8500 Å. This velocity, 2380 km/s (after correcting by the heliocentric velocity of -20 km/s), is equal to the velocity that we infer by symmetrizing the stellar velocity curve with respect to the nucleus. The amplitude of this curve is $\sim \pm 160$ km/s. Typical errors are $\sim$ 30 km/s.

Figure 15 compares the stellar with the ionized gas (traced by [NII] measured in the IFS and Hα measured in the KPNO data) velocity curves at P.A= 6°. Note the asymmetry of the velocity curve of the ionized gas with respect to the nucleus, and the larger amplitude of this curve with respect to the stellar one. This plot also clearly shows that the ionized nuclear gas is blueshifted with respect to the stellar systemic velocity. However, [OIII] nuclear emission blueshifted with respect to the stellar motions is commonplace in Seyfert nuclei (e.g. Nelson & Whittle 1995).

The stellar velocity dispersion along P.A= 6° has been also estimated from the width of the cross-correlation function. Like the velocity dispersion of the ionized gas, the radial distribution of the velocity dispersion also peaks at the position of the nucleus. The stellar velocity dispersion of the nucleus is $\sigma = 260 \pm 20$ km/s, in agreement with the value (σ=220 $\pm$ 25 km/s) estimated by Nelson & Whittle (1995) using the Mgb lines.

4.3. Kinematics of the nuclear ionized gas

The kinematics of the ionized gas in the central 2 arcsec is complex. The [OIII] line shows a very asymmetric profile with a blue wing that extends up to 2 arcsec to the south from the continuum peak. This result was previously reported by Wilson et al (1985). This kinematic structure is fainter in Hβ, but is also detected in our KPNO data in the Hα, [NII] and [SII] lines. At the nucleus (the maximum of the continuum), Hα and [NII] show two velocity components, with the weaker component at redder wavelengths than the brighter one. However, at 2 arcsec south of the nucleus, the weaker component is at bluer wavelengths (Figure 16). We have fitted two gaussians to each line (Hα and [NII]λ6584,6548) to fit the whole profile, and we find that the difference in velocity between these two kinematic components is 250 km/s. We have plotted these two values in the Hα velocity curve (Figure 15) as blue and red circled dots. Note that these components are blue and red shifted with respect to their corresponding radial stellar velocity, suggesting that the central ionized gas is an expanding jet or bubble-like kinematic structure, thus implying that the central gas is out-flowing. This outflow could be caused by the interaction of the radio jet with the circumnuclear gas.

We have visually inspected some [OIII] and Hα+[NII] high resolution STIS spectra (gratings G430M and G750M) that are available in the HST archive (P.I. Whittle and Mundell, respectively). Both data sets have been taken close to the kinematic major axis with a slit width of 0.2 arcsec. These spectra corroborate our results but they also show that the kinematics of the ionized gas at 0.1 arcsec scales is even more complex in detail than provided by the data we present here.

5. Discussion

5.1. Evidence for non-rotational motions in NGC 2110

The ionized gas velocity field in NGC 2110 was obtained by Wilson and Baldwin (1985) on the basis of long-slit spectroscopic observations. They reported a pattern remarkably similar to the rotation curves commonly obtained for spiral galaxies, suggesting that the ionized gas in NGC 2110 was indicating rotation. However, they also reported an interesting asymmetry. Taking the nucleus as reference, the velocities increase more rapidly to the south than to the north. This result led them to suggest that the true kinematic center (i.e. center of rotation) was 1.7 ± 0.4 arcsec towards the south of the optical nucleus. They proposed several alternatives to explain the offset of the kinematic center: a) dust obscuration that hides the true continuum nucleus; b) the ionized gas is not in gravitational motion; c) stars and gas are orbiting in a gravitational potential of a large amount of obscured or dark matter. They dismissed hypothesis (a) because the outer isophotes of the stellar light are not centered on their estimation of the kinematic center. Arguments against hypothesis (b) and in favor of (c) are the description of their velocity curve in terms of a rotation disk. However, for hypothesis (c) to be correct, the interior mass of the nucleus should be $\sim 8{\times}10^9$ $M_\odot$, which is too large to not let a strong signature on the stellar light isophotes. Therefore, they did not find any satisfactory interpretation for the velocity field. Our results indicate that the kinematic center of NGC 2110 is not offset with respect to the optical nucleus, and their hypothesis (b) is correct as we have shown in section 4 and as we further discuss below.

The most clear indication that the warm gas is not just rotating under the galaxy gravitational potential comes from the comparison between its velocity and the stellar velocity along the P.A$= 6°$ (Figure 15). From this figure we infer that: i) the nucleus is indeed at a symmetric position with respect to the stellar kinematics, and ii) the amplitude of the ionized gas velocity curve is larger by 70-90 km/s than the corresponding to the stellar curve. The ionized gas kinematics also support this result. Figures 10 and 13 show the velocity field and the velocity dispersion over NGC 2110 as derived from gaussian fits to the Hα and [NII] emission lines. These maps clearly show the asymmetry reported by Wilson & Baldwin (1985). However, they reveal some features which do not suggest rotation. The asymmetry between the North and South regions of the velocity field is deeper than just the asymmetry in the rotation curve. In the red part the maximum is clearly defined at about 4 arcsec. It is slightly (but significantly) offset from the major photometric axis. The highest velocities in the blue part (North) are found in two regions, each at one side of the photometric major axis. In addition, 'everywhere' in the receding part of the velocity field the velocities change more rapidly than in the corresponding blue region. Moreover, the amplitude of this velocity field (~ 400 km/s) is very large if compared with what is typical for early type galaxies (see, for instance Simien & Prugniel 2000). In addition, the gas velocity dispersion map is elongated along the minor photometric angle, that presumably points to the rotation axis of the galaxy. All this suggests that the motions of the ionized gas do not indicate gravitationally bound orbits, as previously suggested.

To quantify the differences between the ionized gas velocity field with respect to a pure rotation disk, we have built a 2D rotational model using a 1D model fitted to the stellar velocity field. We use equation (2-54c) of Binney and Tremaine (1987):

$$v_c = \frac{v_0 r}{\sqrt{r^2 + r_0^2}} \tag{1}$$

where v_0 is the asymptotic rotational velocity, and r_0 the distance from the kinematic center at which the velocity arises to $v_0/\sqrt{2}$. From a fit to the deprojected stellar velocity curve, we obtain the values of $v_0 = 245$ km/s and $r_0 = 1.85$ arcsec. With these parameters we have built the 2D rotational model, projected to the plane of the sky with an inclination of 42°, the line of nodes at PA=163° and a systemic velocity equal to 2380 km/s (as determined by the stellar rotational curve). The predicted velocity field and the residual map resulting from the subtraction of this rotational disk to the IFS velocity field are plotted in Figure 17. The residual map shows that the nucleus is blue-shifted with respect to the systemic velocity, and there is an excess velocity of up to +100 km/s on the south. The residuals on the north are smaller, less than 30 km/s. Therefore, we have found strong evidence that the ionized gas in the south of NGC 2110 is not following the pure gravitational potential of the galaxy.

5.2. Origin of the out-flowing nuclear ionized gas

The residual velocity map and the kinematic structure found in the strongest nebular lines and the two velocity components in Hα and [NII] indicate that the NLR gas is flowing out of NGC 2110. Additional evidence of an out-flowing gas is the alignment of the maximum of the emission-line widths and the galaxy minor axis. Other examples of outflows in AGNs have been reported previously. In some cases, the outflow is spatially resolved at large scales (e.g. Cecil, Bland & Tully 1990; Colbert et al 1996; Veilleux, Shopbell & Miller 2001; Arribas, Colina & Clements 2001), and in other cases, the outflow is not resolved and it is restricted to the NLR (e.g. Whittle 1985). Several mechanisms can be responsible for the outflow. They are: 1) a thermal wind from a circumnuclear starburst (e.g. Colina, Arribas & Borne 1999); 2) a thermal wind by the AGN torus (Krolik & Begelman 1986); and 3) collimation by a radio jet (Taylor, Dyson & Axon 1992) or entrainment along the radio jet.

We can discard the circumnuclear starburst model as the origin of the outflow in NGC 2110 based on our previous analysis of the nuclear stellar population. The optical continuum distribution and the stellar features do not show any strong evidence of a circumnuclear starburst, except that a small fraction of the optical light could be provided by a young stellar population or by a scattered light from the hidden Seyfert 1 nucleus. Due to the degeneracy in the slope between a power law and a young (≤ 10 Myr) stellar population (see Cid Fernandes & Terlevich 1995) we can not distinguish between these two components. The analysis of the equivalent width of the stellar features (CaII K and G band) presented here (see Figure 9) also indicates that the scattered light (or the young stellar component) has to be extended toward the north of the nucleus. However, in absence of a strong evidence for the existence of a starburst, such as Wolf-Rayet features, high-order Balmer lines in absorption, etc, we interpret this dilution as produced by AGN scattered light.

A detailed analysis of the STIS spectra should distinguish between the other three mechanisms. However, our analysis and the radio morphology of NGC 2110 points out to the collimated jet-driven outflow model as the more plausible mechanism for the nuclear outflow. The radio continuum observations (Ulvestad & Wilson 1983; Nagar et al 1999) have revealed a linear radio structure aligned ± 2 arcsec North-South from the nucleus. Mulchaey et al (1994) have found that the optical emission lines and radio continuum emission extend along similar directions; however, their brightness distributions appear anticorrelated, and the optical jet more curved than the radio jet. Pringle et al (1999) have derived the orientation of the radio jet. They found that the jet is at 50° from the line of sight and 29° with respect to the line of nodes. Therefore, the radio jet is not parallel to the rotational axis. This misalignment suggests that the angular momentum vector of the accretion disk collimating the jet is also misaligned with respect to the host galaxy. However, these angles indicate that the radio jet is pointing toward us and, therefore, it explains the blueshifted velocities observed in the nuclear region as due to a jet induced outflow.

5.3. Origin of the non-rotational motions on the south of the galaxy

Figure 15 indicates that, excluding the nucleus, the stellar and ionized gas velocities fields are in very good agreement towards the North. Towards the South, the disagreement is clear, though the residual velocities (Figure 17b) do not correlate with the ionized gas distribution (Figure 5). Therefore, although the radio jet may play a role to explain the north-south asymmetry in the velocity field of the ionized gas, other mechanism is required to explain why the ionized gas is red-shifted by more than about 100 km/s with respect to the stellar rotation velocity field at the south of the galaxy, and about 240 km/s with respect to the nuclear stellar velocity.

Other evidence that the velocity field at the south is peculiar has been reported by Gallimore et al (1999). HI observations with the VLA have detected an HI cloud in absorption, located south of the maximum of the radio continuum emission. This cloud has a velocity of 2626 km/s and, therefore, it is red-shifted about 246 km/s with respect to the nuclear stellar systemic velocity. Gallimore et al have interpreted this HI absorption as a rotational disk of HI. They argue that we may not see the HI disk in the North because the North radio jet is in front of the disk as seen by us; at the South, the radio jet is behind the disk illuminating it. However, this HI velocity agrees very well with the velocity of the ionized gas that we measure at the south of the galaxy, both thus having an excess +100 km/s with respect to the pure rotation at that radius. Therefore, an alternative explanation is that an HI cloud is infalling toward the galaxy and it is impacting close to the center of NGC 2110.

The decoupling between the ionized gas and the stellar velocities could be explained if a minor merger is occurring in NGC 2110. The fact that the morphology at large scales is not perturbed (we don't see distortion of the isophotal contours or evidence of tidal tails), indicates that it would have to be a minor-merger with a small galaxy or an intergalactic HI cloud, that does not produce a strong effect on the large scale morphology of the galaxy. This is supported by previous studies of the effects of a minor merger in a main galaxy. From a detailed study of a sample of nearby Sa galaxies, Haynes et al (2000) and Haynes (2001) find that while these galaxies show no morphological signs of interaction, they do show a range of clear kinematical peculiarities that can be interpreted in terms of a kinematic memory of a past minor merger. A similar conclusion is also bore by numerical simulations of minor merger accretion by early type galaxies (Bak 2000); Bak concludes that there is no major photometric distinction between galaxies which have undergone a minor merger and those which have not.

To investigate the minor-merger hypothesis as the origin of the red-shifted HI absorption line and the excess of the ionized gas red-shifted velocity at the south of the nucleus, we have further inspected the HST images to look for fine detail morphological peculiarities in the center of the galaxy. An un-sharp masked F606W image (Figure 18) reveals some morphological features that have not been detected previously in the I and Hα images. Besides the dust lanes that trace a spiral pattern toward the nucleus which are common in HST images of galaxies (e.g. Pogge & Martini 2002), there are some residual arcs in emission at a radius of 6 to 8 arcsec located south to north-east to north of the nucleus. In addition, there are also some *radial* dust lanes. Note that while the more typical spiraling dust lanes are located mostly to the north-west side (and south at small radii), these *radial* dust lanes are mostly located at the south-east to south-west quadrants (at larger radii), in particular, the most prominent of these lanes is at the south-west pointing directly to the HI cloud.

These features are very faint and they do not affect the large scale symmetry in the isophotal analysis, in agreement with the findings of Haynes (2001) and Bak (2000). A possible interpretation is that these faint features and kinematic peculiarities in the south of the galaxy are produced by a minor-merger with a small satellite or intergalactic HI cloud that passed through in a highly inclined orbit close to the nucleus of NGC 2110. Merger or passage of larger satellite galaxies do produce similar spoke-like structures, but at significantly larger scales, that are very clearly reflected on the overall morphology of the galaxy (such as, e.g., the Cartwheel). Very detailed analysis of faint structures are needed to find more such little mass encounter candidates.

Thus, if the interpretation of these morphological and kinematic peculiarities is correct, we are observing a case in which the nuclear activity could be driven by a minor merger. Taniguchi (1999) has proposed that the fueling mechanism of isolated non-barred Seyfert galaxies could be due to a minor-merger between a disk galaxy and a nucleated satellite. If the major galaxy has a gas-poor disk, then, Seyfert activity without circumnuclear star formation is triggered. Even more, he suggests that the plane of the accretion disk that forms is parallel to the galaxy rotation disk if the satellite impacts the disk with an almost aligned orbit. On the contrary, when the satellite impacts almost perpendicular to the disk, a Seyfert 2 can form with the plane of the accretion disk highly inclined with respect to the rotational disk of the host galaxy. This scenario gives also a plausible explanation for the misalignment between the orientation of the radio jet and the galaxy rotation axis of NGC 2110.

Thus, we suggest that the morphological and kinematic peculiarities seen in the south of NGC 2110 could be produced by a minor-merger of the galaxy with a nucleated satellite that impacts the disk of NGC 2110 close to its nucleus with a highly inclined orbit. We speculate that this could be the mechanism responsible of triggering the Seyfert activity in this isolated non-barred Sa galaxy, that drive the gas toward the center to feed the AGN.

6. Summary and conclusions

We have obtained Integral field optical spectroscopy in the range 3700-7000 Å, and long-slit optical spectroscopy (3400-5500 Å and 6600-9100 Å) along P.A= 6° of the Seyfert 2 galaxy NGC 2110. These observations allow us to get the distributions of the emission lines (Hα, Hβ, [OIII], [OI], [NII], and [SII]), the ionized gas velocity field, the velocity dispersion map, and the stellar velocity curve along P.A=6°. These data combined with HST+WFPC2 (I, F606W and Hα) have reported the following results:

- At large scales, the morphology of NGC 2110 is not perturbed. The red continuum is well fitted by ellipses that have their major axis oriented at P.A=163.5°, and an inclination of 42°. The centers of these ellipses are located at the maximum of the continuum within 0.13 arcsec in RA and 0.07 arcsec in Dec. This result indicates that the photometric center is at the nucleus of the galaxy.

- V and I un-sharp masked images have revealed dust lanes that spiral toward the nucleus and they may represent the gas flows that feed the AGN. The V (F606W) un-sharp masked image shows also radial dust lanes and emission arcs at 5 and 8 arcsec at the south and north-east, similar to the tidal debris predicted by numerical simulations of the merger of a small galaxy with a galaxy disk.

- The ionized gas is extended in the North-South direction, such as the linear radio jet. The morphology of [OI], [NII] and [SII] is similar to [OIII], that is more extended to the north than to the south. This distribution suggests that the gas at the north may be photoionized by the AGN. At larger scales, Hα and Hβ images show an S-shape that is similarly extended at the north and at the south.

- The ionized velocity field shows clearly a north-south asymmetry, with a larger velocity gradient in the south than in the north. This asymmetry is seen also along the kinematic major axis. This result suggests that the ionized gas is not normally rotating gas in the disk of the galaxy. The ionized [NII] nuclear gas velocity is 2315 km/s.

- The ionized gas velocity dispersion map shows a bar like morphology oriented near the photometric minor axis. The maximum of the velocity dispersion is also coincident with the maximum of the optical continuum. Thus, the kinematic center is coincident with the nucleus of NGC 2110. This alignment between the maximum of the emission line widths and the galaxy minor axis may be due to a wind driven by the AGN.

- The stellar velocity curve inferred from the CaII triplet observed along P.A=6° is symmetric with respect to the nucleus that has a systemic velocity of 2380 km/s. The amplitud of the stellar velocity curve is lower than the amplitud of the ionized gas velocity curve.

- The nuclear ionized gas of NGC 2110 is blueshifted with respect to the stellar systemic velocity. Two velocity components that are shifted $\pm$125 km/s from the stellar rotation curve have been detected at the central 2 arcsec. These components indicate that the NLR is out-flowing, possibly driven by the radio jet.

- At larger spatial scales (up to 5 arcsec), the ionized gas on the south of NGC 2110 is red-shifted by about 100 km/s with respect to the stellar velocity field, and 240 km/s with respect to the nuclear stellar systemic velocity. This excess of the velocity with respect to the rotation indicates that the gas in the south of NGC 2110 is not following the pure gravitational potential of the galaxy. It is coincident with the HI red-shifted (240 km/s) absorption extended to the south of the nucleus detected by Gallimore et al (1999).

We conclude that the ionized gas on the south is kinematically perturbed. This conclusion together with the morphological peculiarities detected (arcs, radial dust lanes) suggests that the nuclear activity could be the result of a minor-merger. The collision with a nucleated small satellite (or with an intergalactic HI cloud) with a very high inclined orbit that impacts close to the nucleus may be responsible of the red-shifted velocity of the ionized gas in the south of the galaxy and the arcs and radial dust lanes observed in the central host disk of the galaxy. This interpretation of the data is of relevance in relation with the fueling mechanism and the triggering of nuclear activity in isolated non-barred Seyfert galaxies.

Acknowledgments

We are grateful to Jack Gallimore, the referee, for his suggestions and corrections that helped to inprove the paper. We also thanks to Luis Cuesta for making his *inter2r* program available that allows to built the two-dimensional images, Jaime Perea for SIPL, and Luis Colina for his comments from a thorough reading of the paper. This work was supported by the Spanish DGICYT project AYA2001-3939-C03-01.

The 4.2m William Herschel Telescope is operated by the Isaac Newton Group at the Observatorio de Roque de los Muchachos of the Instituto de Astrofísica de Canarias.

Based observations made with the NASA/ESA Hubble Space Telescope, obtained from the data archive at ST-ECF.

REFERENCES

Adams, T.F. 1977, ApJS, 33, 19

Athanassoula, R. 1992, MNRAS, 259, 345

Arribas, S., Mediavilla, E., García-Lorenzo, B., del Burgo, C. 1997, ApJ, 490, 227

Arribas, S., et al. 1998, Proc. SPIE, 3355, 821

Arribas, S., Colina, L. & Clements, D., 2001, ApJ, 560, 160

Bak, J., 2000, PhD thesis, Ohio University

Bingham, R.G., Gellatly, D.W., Jenkins, C.R., & Worswick, S.P. 1994, Proc. SPIE, 2198, 56

Binney, J.B., & Tremaine, S.T., 'Galactic Dynamics', 1987, Princeton University Press. Pinceton: New Jersey

Bradt, H.V., Burke, B.F., Canizares, C.R., Greenfield, P.E., Kelly, R.L., McClintock, J.E., van Paradijs, J. & Koski, A.T. 1978, ApJ, 226, L111

Canalizo, G. & Stockton, A. 2001, ApJ, 555, 719

Cecil, G., Bland, J. & Tully, R.B. 1990, ApJ, 355, 70

Cid Fernandes, R. & Terlevich, R. 1995, MNRAS, 272, 423

Cid Fernandes, R., Heckman, T., Schmitt, H.R, González Delgado, R.M & Storchi-Bergmann, T. 2001, ApJ, 558, 81

Colbert, E.J.M., Baum, S.A., Gallimore, J.F., O'Dea, C.P., Lehnert, M.D., Tsvetanov, Z.I., Mulchaey, J.S. & Caganoff, S. 1996, ApJS, 105, 75

Colina, L., González Delgado, R.M., Mas-Hesse, J.M. & Leitherer, C. 2002, ApJ, submitted

Colina, L., Arribas, S. & Borne, K.D, 1999, ApJ, 527, L13

de Vaucouleurs, G., de Vaucouleurs, A., Corwin, JR. H.G, Buta, R.J., Paturel, G. & Fouqué, P. 1991, Third Reference Catalogue of Bright Galaxies (Austin: Univ. of Texas) (RC3)

Dahari, O. 1984, AJ, 89, 966

De Robertis, M.M., Yee, H.K.C. & Hayhoe, K. 1998, ApJ, 496, 93

Ferruit, P., Wilson, A.S., Whittle, M., Simpson, C., Mulchaey, J.S. & Ferland, G.J. 1999, ApJ, 523, 147

Gallimore, J.F, Baum, S.A., O'Dea, C.P., Pedlar, A. & Brinks, E. 1999, ApJ, 524, 684

García-Lorenzo, B., Mediavilla, E., Arribas, S. & del Burgos, C., 1997, ApJ, 483, L99

García-Lorenzo, B., Mediavilla, E., & Arribas, S. 1999, ApJ, 518, 190

González Delgado, R.M. 2001, in *Issues in Unification of AGNs*, in press (astro-ph/0109505)

González Delgado, R.M., Heckman, T. , Leitherer, C., Meurer, G., Krolik, J., Wilson, A.S., Kinney, A. & Koratkar, A. 1998, ApJ, 505, 174

González Delgado, R.M., Heckman, T. & Leitherer, C. 2001, ApJ, 546, 845

Haynes, M.P., Jore, K.P., Barrett, E.A., Broeils, A.H., Murray, B.M. 2000, AJ, 120, 703

Haynes, M.P., in 'Gas and galaxy Evolution', 2001, ASP Conf. vol. 240, p. 257

Heckman, T.M., González-Delgado, R., Leitherer, C., Meurer, G.R., Krolik, J., Kinney, A., Koratkar, A., & Wilson, A.S. 1997, ApJ, 482, 114

Hunt, L., Malkan, M.A., Salvati, M., Mandolesi, N., Palazzi, E, & Wade, R. 1997, ApJS, 108, 229

Knapen, J.H., Shlosman, I. & Peletier, R. F. 2000, ApJ,529, 93

Knop, R.A., Armus, L., Matthews, K., Murphy, T.W. & Soifer, B.T. 2001, ApJ, 122, 764

Krolik, J.H. & Begelman, M.C. 1986, ApJ 308, L55

Lehnert, M.D. & Heckman, T.M. 1996, ApJ, 462, 651

Lutz, D. & Tacconi, L.J. 1999, in *Ultraluminous galaxies: monsters or babies*, ed. D. Lutz & L.J. Tacconi, Astrophysic & Space Science, 266

Maiolino, R., Risaliti, G. & Salvati, M. 1998, A&A, 341, L35

Malkan, M.A., Varoujan, G. & Raymond, T. 1998, ApJS, 117, 25

Márquez, I., Durret, F., Masegosa, J., Moles, M., González Delgado, R.M., Marrero, I., Maza, J., Pérez, E. & Roth, M. 2000, A&A, 360, 431

Martini, P. & Pogge, R.W. 1999, AJ, 118, 2646

McClintock, J.E., van Paradijs, J., Remilliard, R.A., Canizares, C.R., Koski, A.T. & Veron, P. 1979, ApJ, 233, 809

Mihos, J.C., & Hernquist, L. 1996, ApJ, 464, 641

Moles, M., Márquez, I. & Pérez, E. 1995, ApJ, 438, 604

Mulchaey, J.S. & Regan, M. 1997, ApJ, 482, L135

Mulchaey, J.S. & Regan, M. 1999, AJ, 117, 2676

Mulchaey, J.S., Wilson, A.S., Bower, G., Heckman, T.M., Krolik, J.H. & Miley, G.K. 1994, ApJ, 433, 625

Mundell, C.G., Wilson, A.S., Ulvestad, J.S., & Roy, A.L. 2000, ApJ, 529, 816

Nagar, N.M., Wilson, A.S., Mulchaey, J.S. & Gallimore, J.F. 1999, ApJS, 120, 209

Nelson, C., & Whittle, M. 1995, ApJSS, 99, 67

Noguchi, M. 1988, A&A, 203, 259

Pogge, R.W. 1989, ApJ, 345, 730

Pogge, R.W. & Martini, P. 2002, ApJ, 569, 624

Pringle, J.E., Antonucci, R.R.J., Clarke, C.J., Kinney, A.L., Schmitt, H.R. & Ulvestad, J.S. 1999, ApJ, 526, L9

Quillen, A.C., Alonso-Herrero, A., Rieke, M.J., Falcke, H. & Rieke, G.H. 1999, ApJ, 525, 685

Rafanelli, P., Violato, M. & Baruffolo, A. 1995, AJ, 109, 1546

Regan, M.W. & Mulchaey, J.S. 1999, AJ, 117, 2676

Sanders, D.B., Soifer, B.T., Elias, J.H., Neugebauer, G. & Matthews, K. 1988, ApJ, 328, L35

Shlosman, I., Begelman, M.C. & Frank, J. 1990, Nature, 345, 679

Shuder, J.M. 1980, ApJ, 240, 32

Simien, F. & Prugniel, Ph. 2000, A&AS, 145, 263

Storchi-Bergmann, T., Winge, C., Ward, M.J. & Wilson, A.S. 1999, MNRAS, 304, 35

Strauss, M.A., Huchra, J.P., Davis, M., Yahil, A., Fisher, K.B. & Tonry, J. 1992, ApJS, 83, 29

Taniguchi, Y. 1999, ApJ, 524, L65

Taylor, D., Dyson, J.E., & Axon, D.J. 1992, MNRAS, 255, 351

Tonry, J. & Davis, M. 1979, AJ, 84, 1511

Ulvestad J.S. & Wilson, A.S. 1983, ApJ, 264, L7

Veilleux, S. 2001, in *Starbursts Near and Far*, eds. Tacconi, L. & Lutz, D. (Springer-Verlag), SSP 88, 88

Veilleux, S., Shopbell, P.L. & Miller, S.T. 2001, ApJ, 121, 198

Weaver, K.A., Mushotzsky, R.F., Serlemitsos, P.J., Wilson, A.S., Elvis, M. & Briel, U. 1995, ApJ, 442, 597

Whittle, M. 1985, MNRAS, 213, 1

Wilkins, T.N. & Axon, D.J., 1991, TWODSPEC, Starlink User Note, No. 16.

Wilson, A.S. & Baldwin, J.A., 1985, ApJ, 289, 124

Wilson, A.S., Baldwin, J.A. & Ulvestad, J.S. 1985, ApJ, 291, 627

Zaristky, D., Smith, R., Frenk, C. & White, S.D.M. 1997, ApJ, 478, 39

This preprint was prepared with the AAS LaTeX macros v5.0.

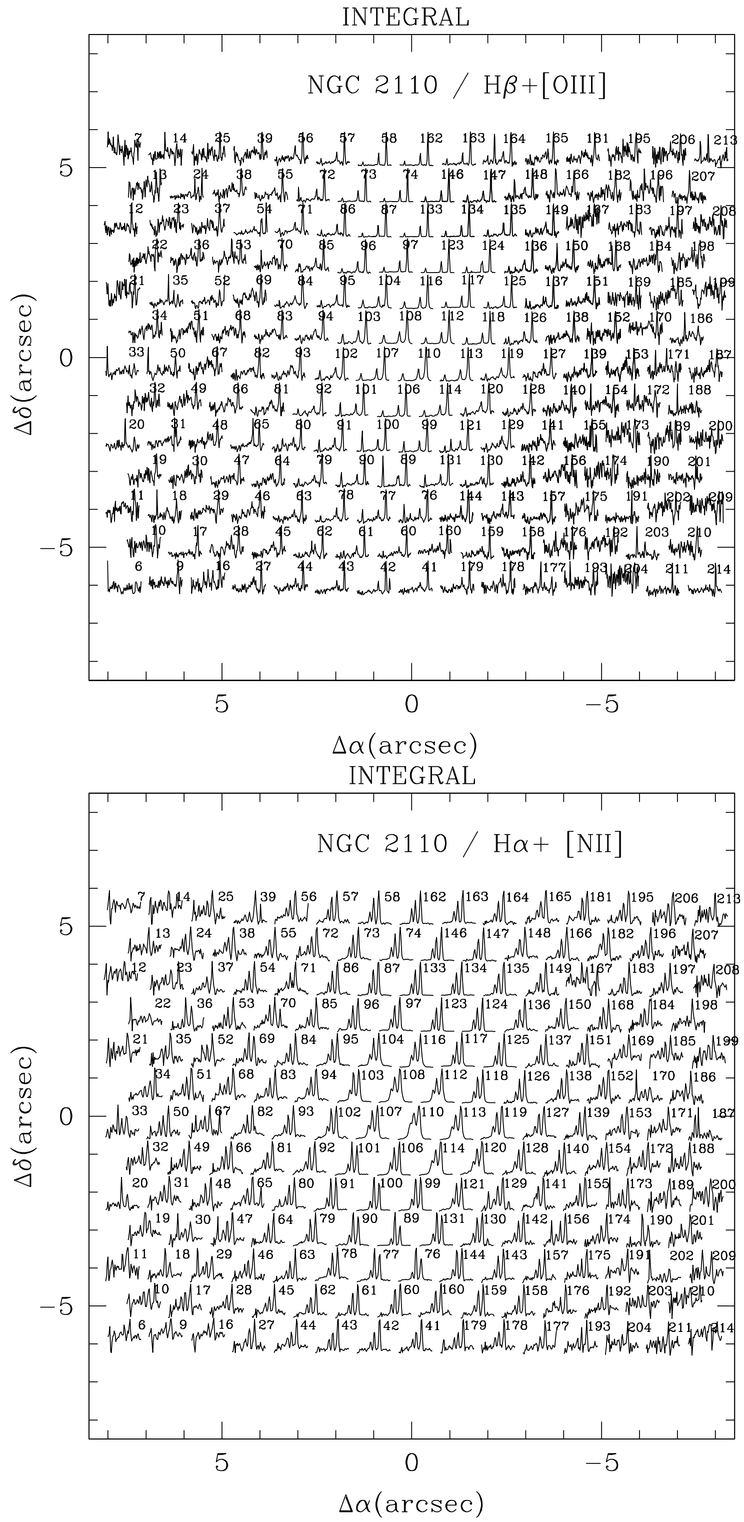

Fig. 1.— Final calibrated circumnuclear (16.5×12.3 arcsec) spectra of NGC 2110 in the spectral ranges: (a) λ4870-5080 including Hβ, [OIII] λ 4959, 5007; (b) λ6650-6685 including Hα, [NII] λ 6548, 6584. The numbers in the plot indicate the number of the fiber at the entrance of the spectrograph. The orientation is North up and East left. The 180 spectra are autoscaled.

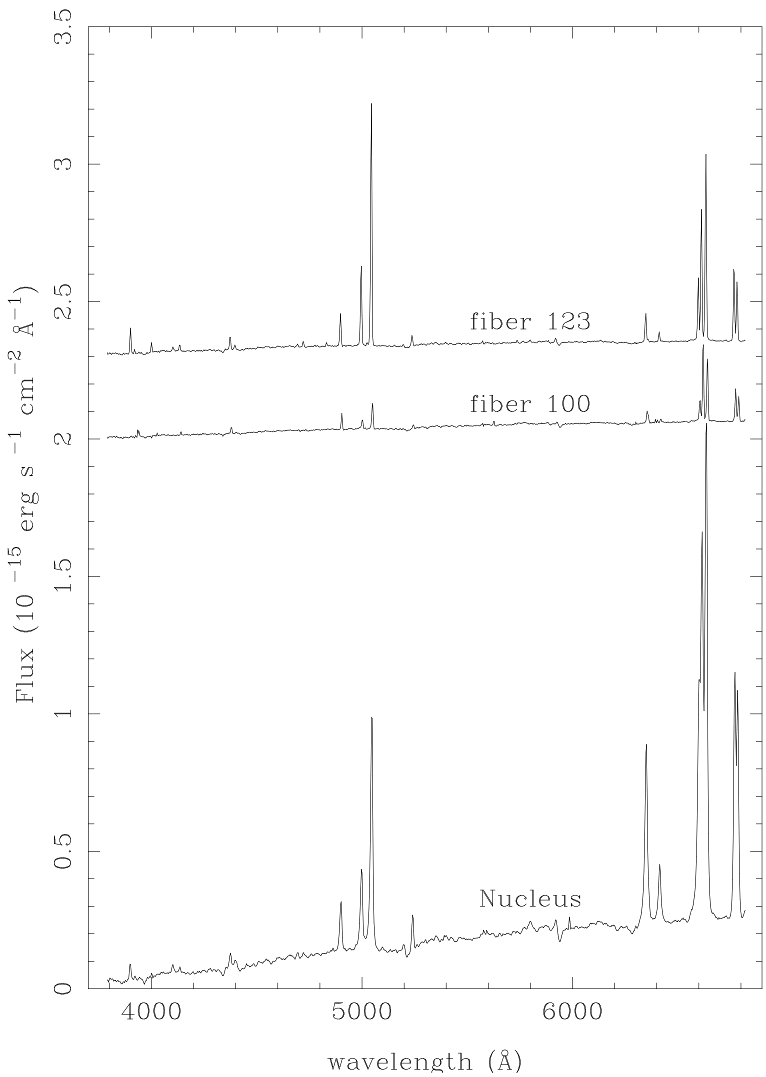

Fig. 2.— Nuclear and two circumnuclear spectra of NGC 2110, corresponding to the fibers 110 (nucleus), 100 ($\sim$ 2 arcsec south of the nucleus) and 123 ($\sim$ 3 arcsec north of the nucleus). The circumnuclear spectra are shifted by 2 and $2.3{\times}10^{-15}$ erg s^{-1} cm^{-2} Å^{-1}. Note the strong gradient along the excitation in the north-south direction.

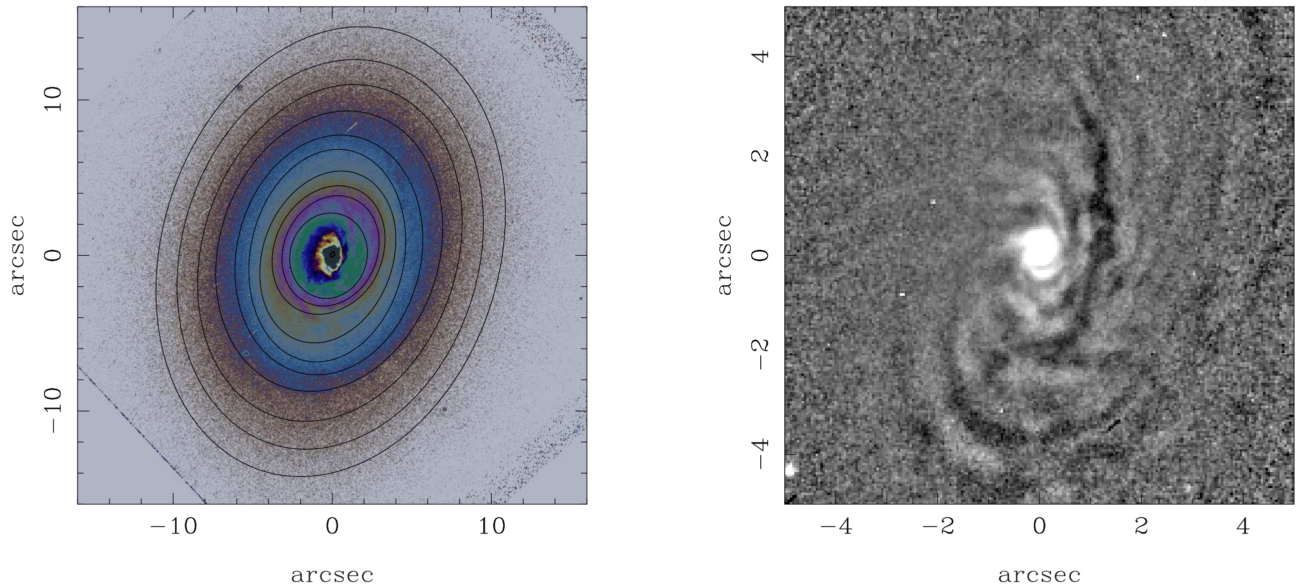

Fig. 3.— HST+WFPC2 (PC) images of NGC 2110: a) In grey scale is the continuum emission through the filter F791W. Over-plotted as full lines are the isophotal contours fitted to this image. b) Unsharp masked image. Dust lanes trace a spiral patern around the nucleus to the nucleus are clearly seen at 1 and 2 arcsec to the west. North is up and East to the left. This is the orientation in all the images.

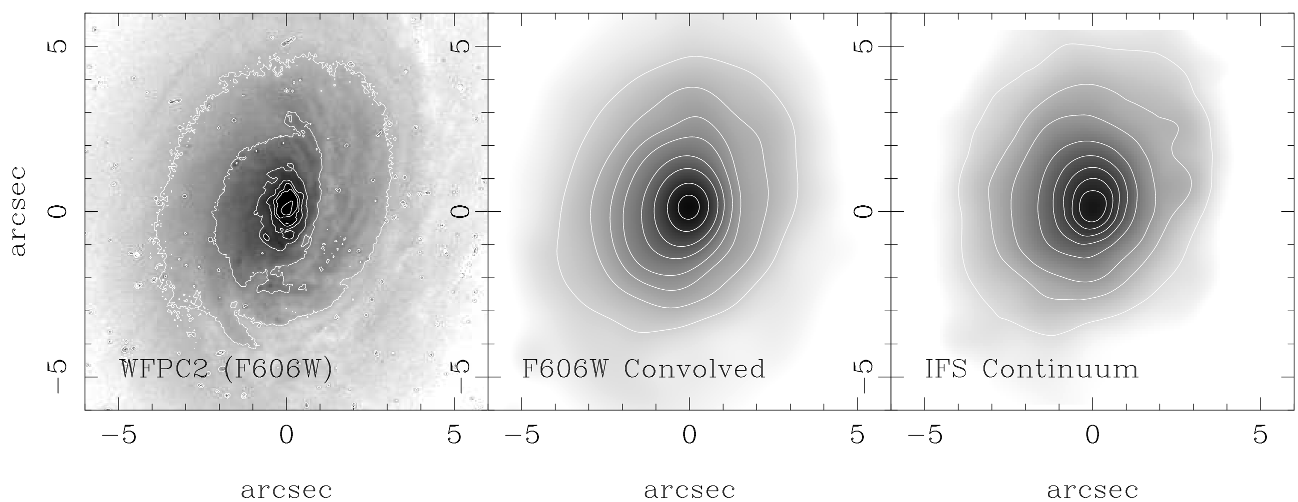

Fig. 4.— a) HST+WFPC2 image of the central light distribution of NGC 2110 through the filter F606W. b) F606W image convolved with a gaussian with a σ=mean seeing. c) IFS image of the stellar light distribution in the central region of NGC 2110 traced by a continuum window centered at 5380 Å.

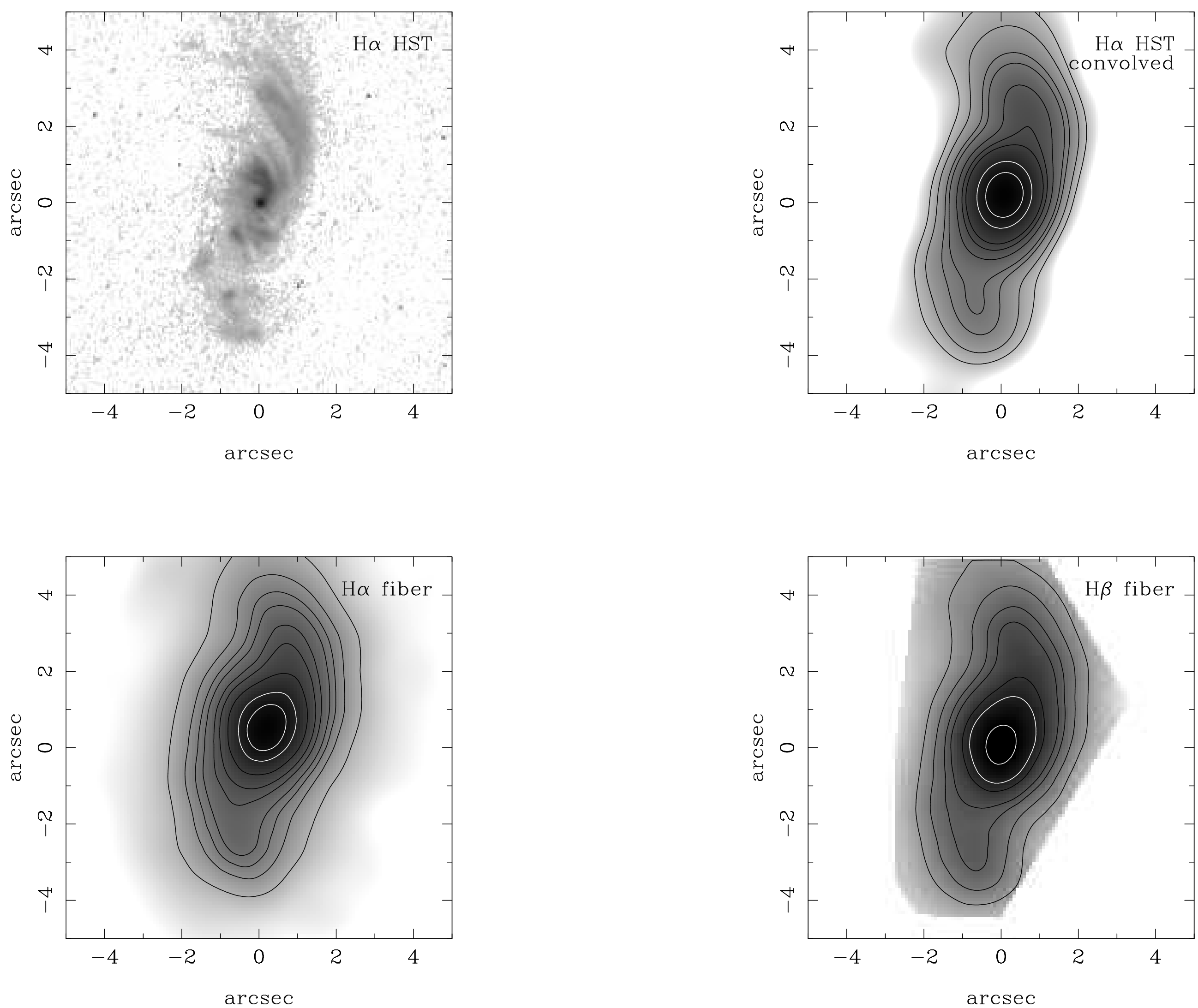

Fig. 5.— a) HST Hα image. b) HST-Hα image convolved with a gaussian of fwhm equal to the mean of our IFS data. c) IFS Hα image. d) IFS Hβ image.

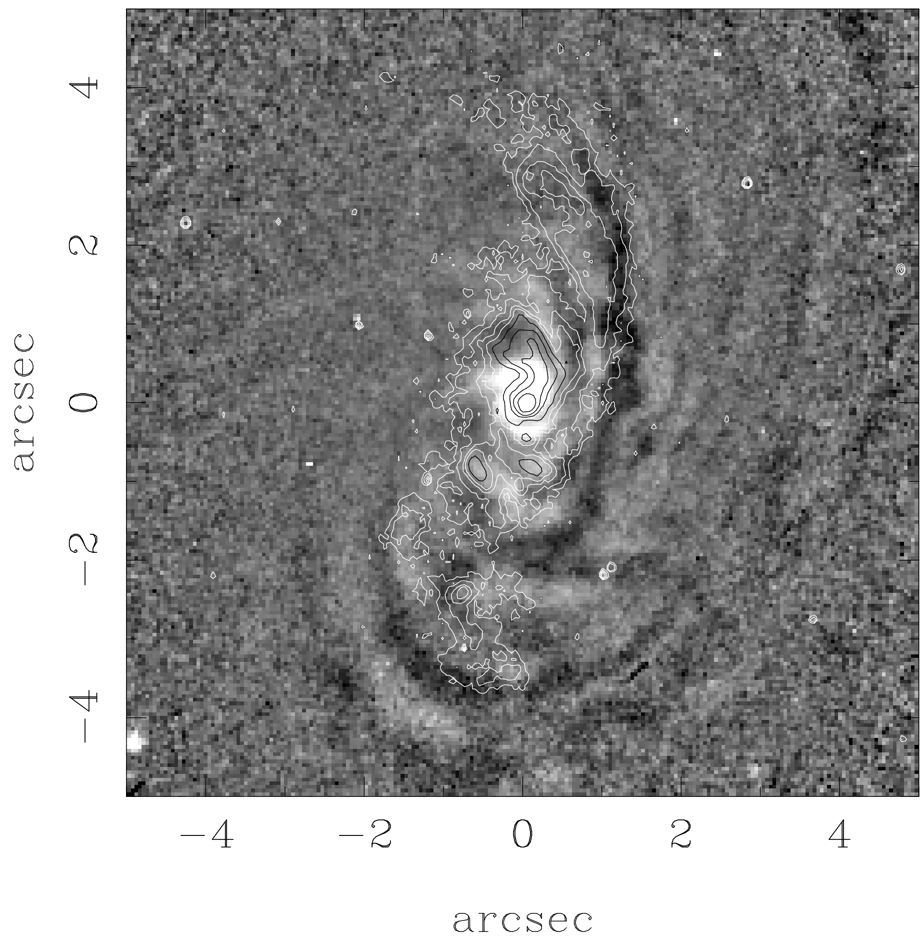

Fig. 6.— The un-sharp masked I image is plotted in grey scale. The contours correspond to the HST-Hα image.

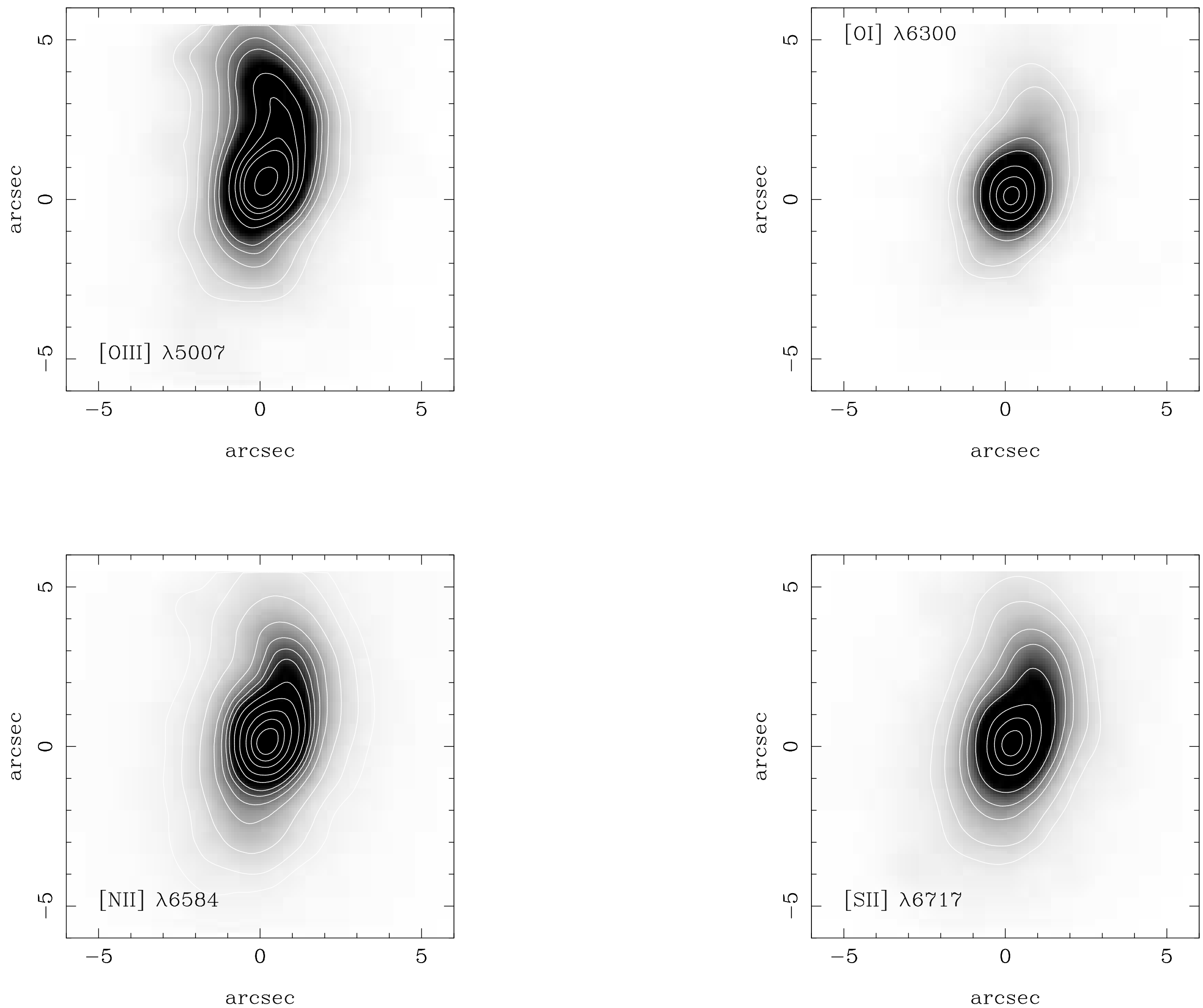

Fig. 7.— INTEGRAL images of the ionized gas circumnuclear region of NGC 2110 as traced by (a) [OIII] λ5007, (b) [OI] λ6300, (c) [NII] λ6584, (d) [SII] λ6717, 6731. The contours correspond to: (a) 3, 5, 10,15, 20, 40, 60, 80, 100, 150, 250 and 300 $\times$ 10^{-15} erg s^{-1} cm^{-2}; (b) 3, 5, 15, 25, 50, 75 and 100 $\times$ 10^{-15} erg s^{-1} cm^{-2}; (c) 3, 5, 10, 20, 30, 40, 50, 70, 100, 150, 200, 250 and 300 $\times$ 10^{-15} erg s^{-1} cm^{-2}; (d) 3, 5, 10, 15, 25, 50, 75 and 100 $\times$ 10^{-15} erg s^{-1} cm^{-2}.

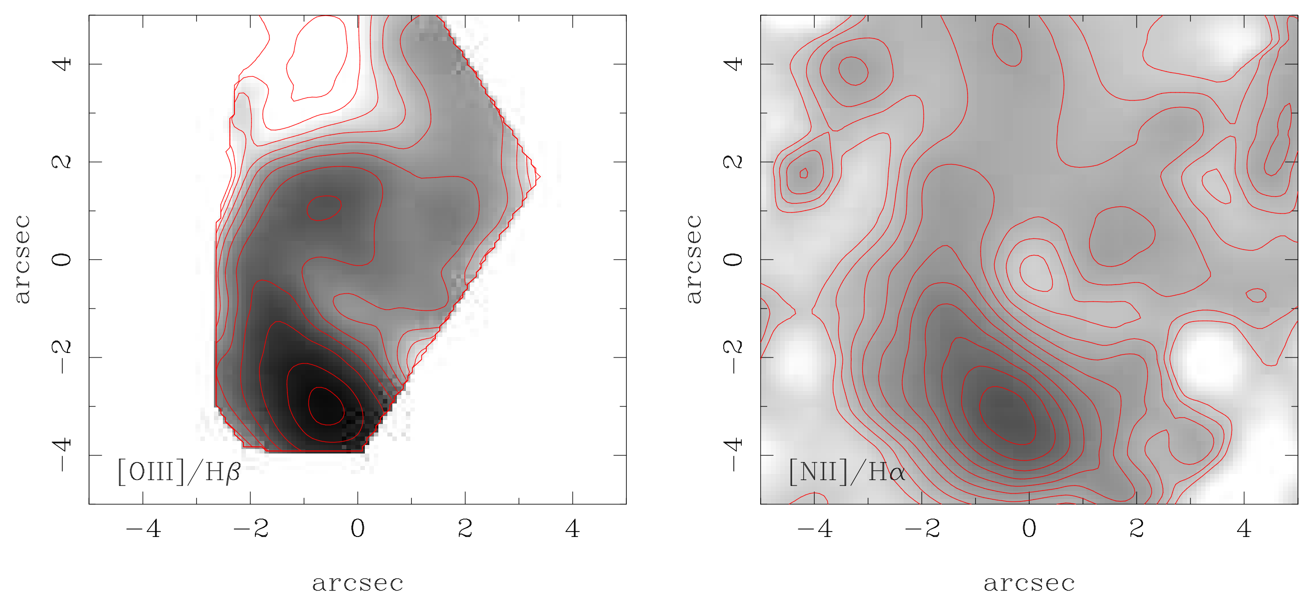

Fig. 8.— INTEGRAL images of the excitation of the ionized gas in the circumnuclear region of NGC 2110 as traced by (a) [OIII] λ5007/Hβ, (b) [NII] λ6584/Hα. Contours correspond to: (a) 1.5 2 3 4 5 6 7 8 9 10 11; (b) 0.7 0.8 0.9 1 1.1 1.2 1.3 1.4 1.5 1.6.

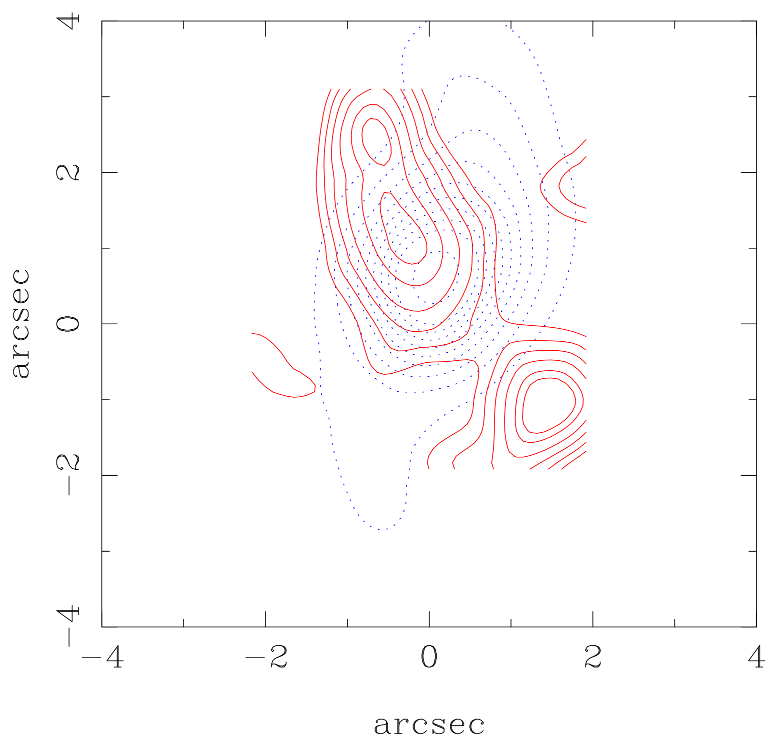

Fig. 9.— Iso-contours (full line) of the equivalent width of the absorption line CaII K measured in the individual spectra over the Hβ emission line distribution (dotted line). The contours plotted have equivalent width of 11.2, 11.5, 12, 12.5, 13, 13.5 Å. The equivalent width decreases inwards, the inner countor corresponds to 11.2 Å.

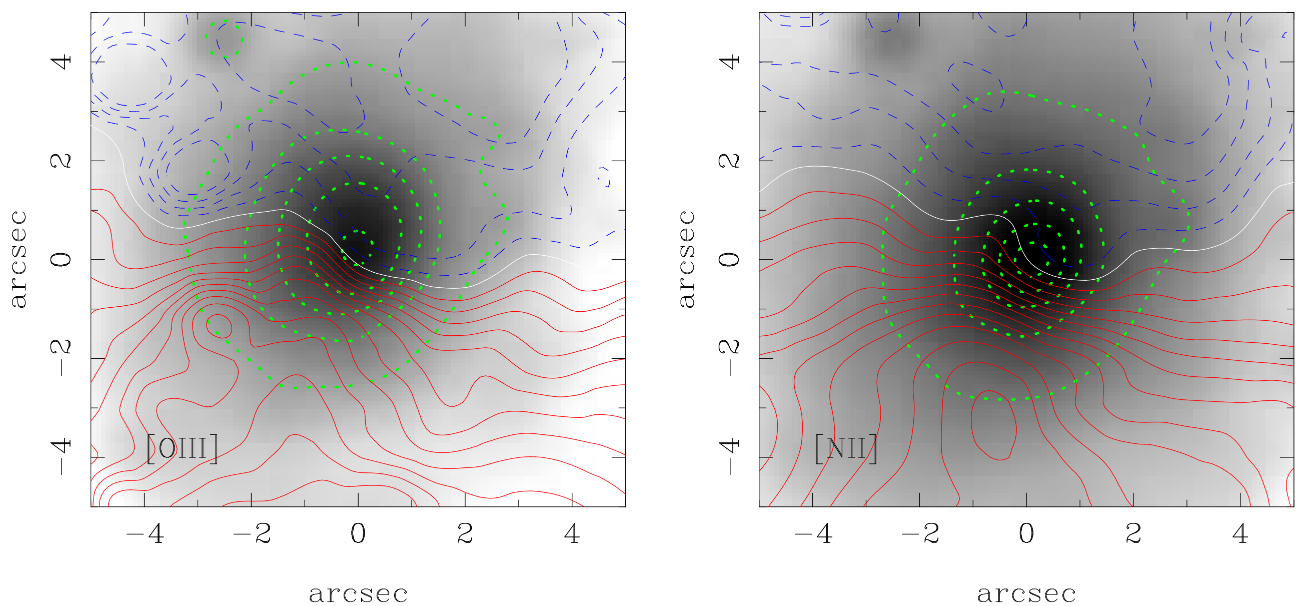

Fig. 10.— Velocity field of the ionized gas in the central region of NGC 2110 inferred from a single gaussian profile fit to the emission lines (a) [OIII] λ5007 and (b) [NII] λ6584. Continuum light is also plotted by gray scale and by contours in green (dotted line). Iso-velocity lines are plotted in steps of 25 km/s. Blue (dashed line) contours are velocity values below 2315 km/s, and red (full line) are velocity values larger than 2315 km/s. The iso-velocity contour of 2315 km/s is plotted by a white full line.

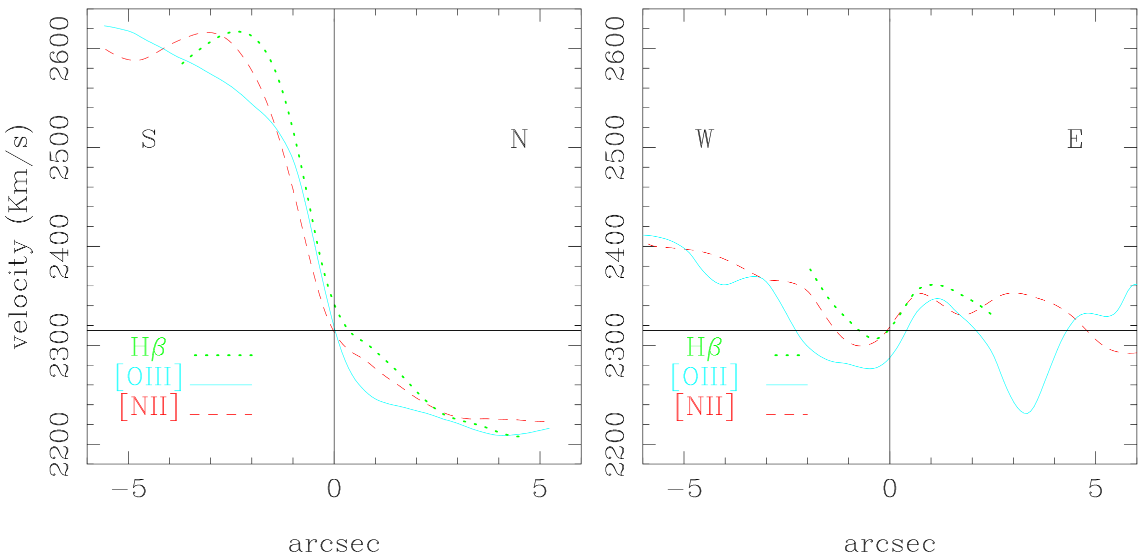

Fig. 11.— Velocity curve of the ionized gas traced by Hβ (dotted green line), [OIII] (full blue line) and [NII] (dashed red line) obtained from cuts in the INTEGRAL velocity fields along the major (left) and minor (right) photometric angle.

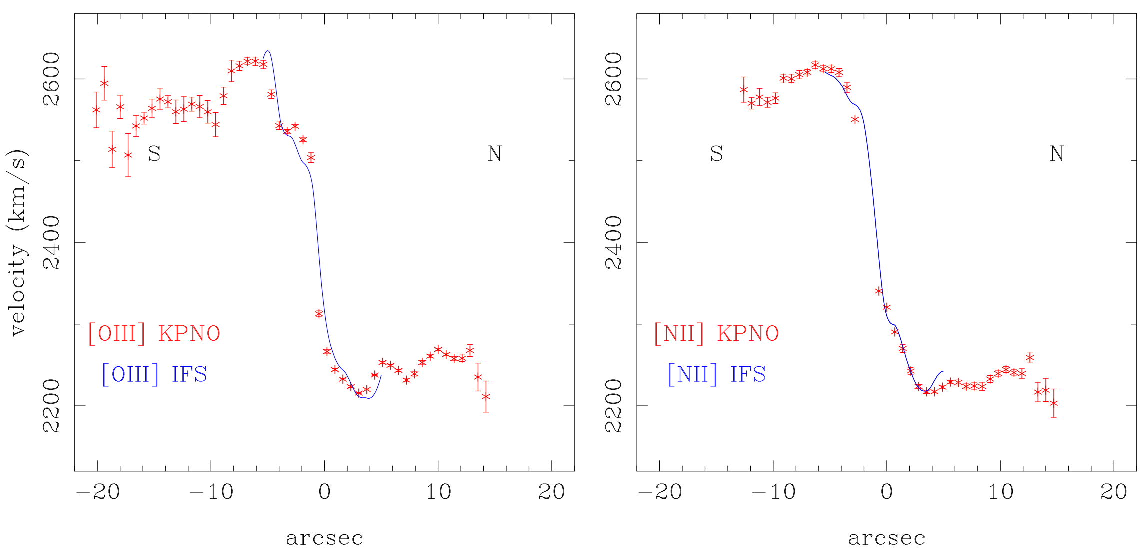

Fig. 12.— Comparison of the velocity curve of the ionized gas obtained from the KPNO data (red cross) and a cut on the IFS velocity field along P.A= 6° (blue line). Velocity curves for [OIII] are on the left and on the right is for [NII].

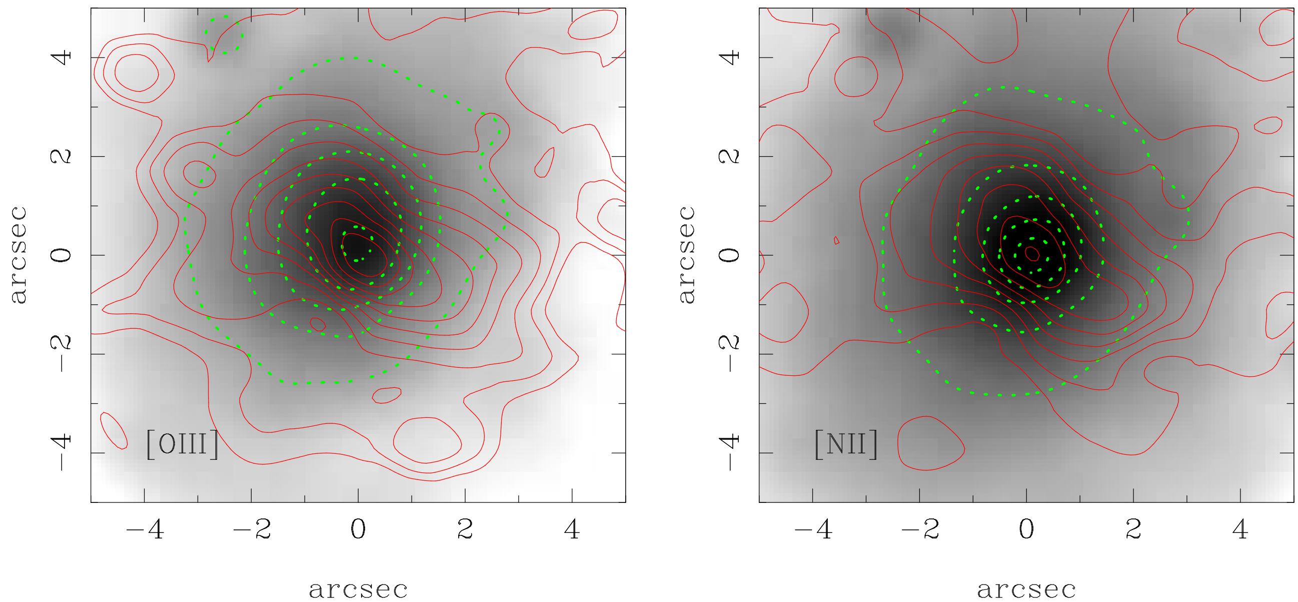

Fig. 13.— Velocity dispersion of the ionized gas in the central region of NGC 2110 inferred from a single gaussian profile fit to the emission lines (a) [OIII] λ5007 and (b) [NII] λ6584. Continuum light is also plotted by greyscale and by contours in green (dotted line). Iso-sigma velocity dispersion is plotted in steps of 20 km/s with the minimuum contour of 100 km/s, and the maximuum of 340 and 240 km/s for [OIII] and [NII], respectively.

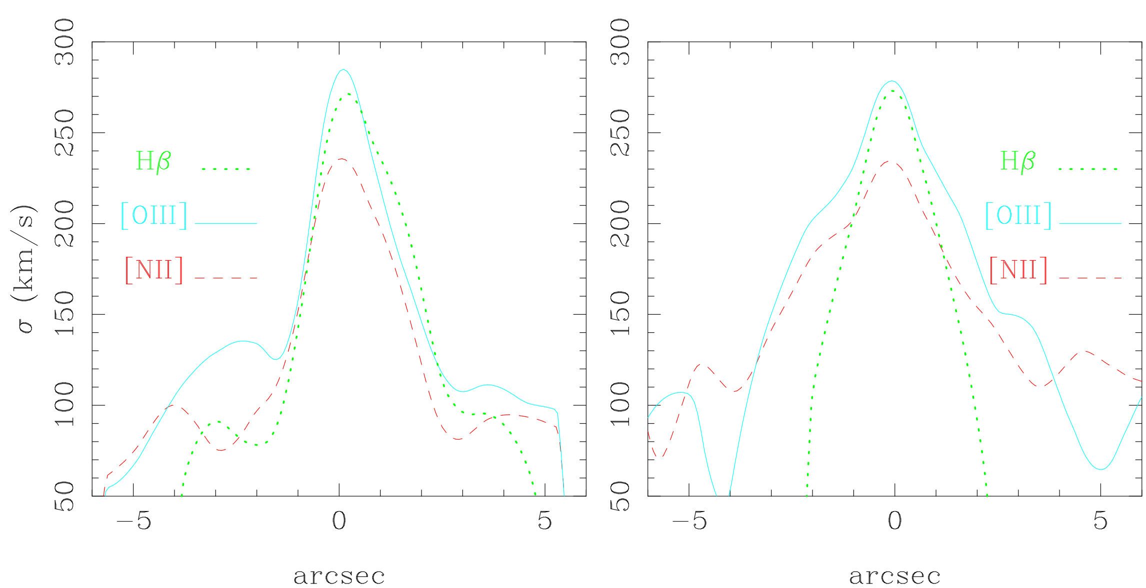

Fig. 14.— As Figure 11 for the ionized gas velocity dispersion.

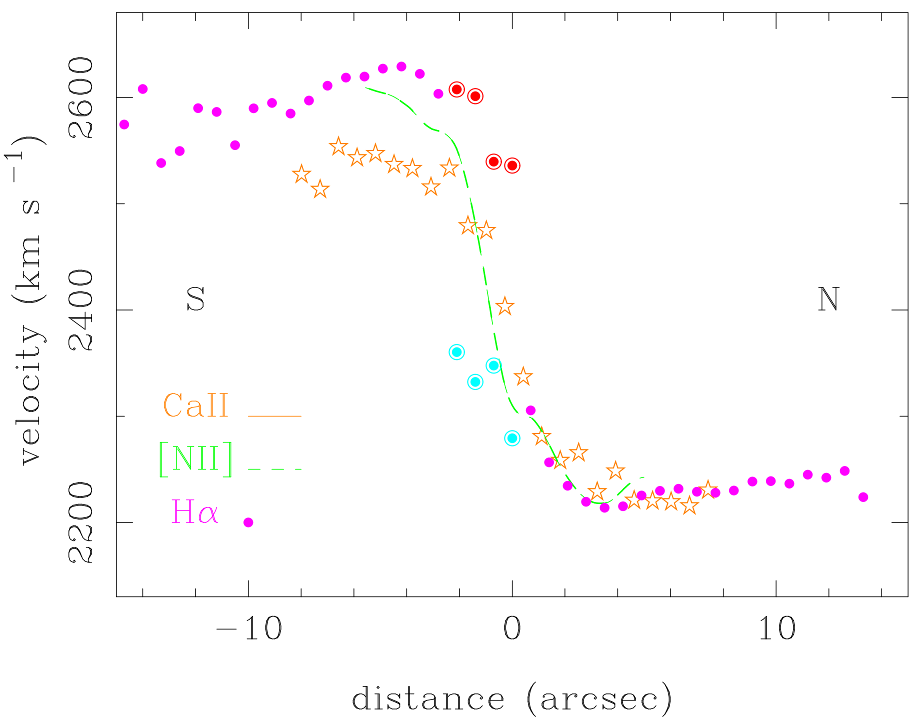

Fig. 15.— Comparison of the stellar velocity curve (orange stars) along the PA=6° inferred from the cross-correlation in the spectral range of the CaII triplet with the velocity curve of the ionized gas traced by the emission line [NII] (green dashed line) inferred from a cut on the velocity field map (figure 7a) along PA=6° and the velocity curve of Hα (dots and circled dots) obtained from the KPNO data. The circled dots represent the two kinematic components fitted to the Hα line.

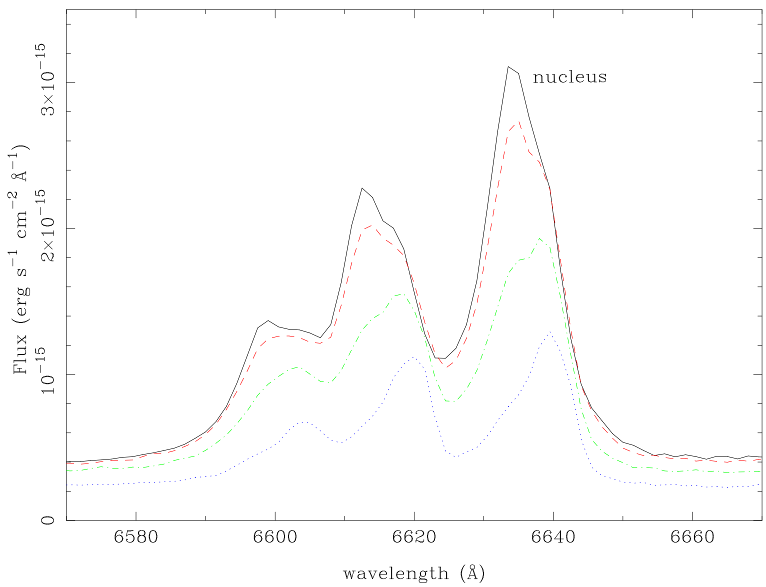

Fig. 16.— Profile of the Hα, and [NII]λ6548,6584 lines in the KPNO data for the crossection where the continuum is maximum (nucleus) and the three next crossections to the south. The spatial sampling is 0.7 arcsec/pixel. The difference in velocity between the two components is about 250 km/s.

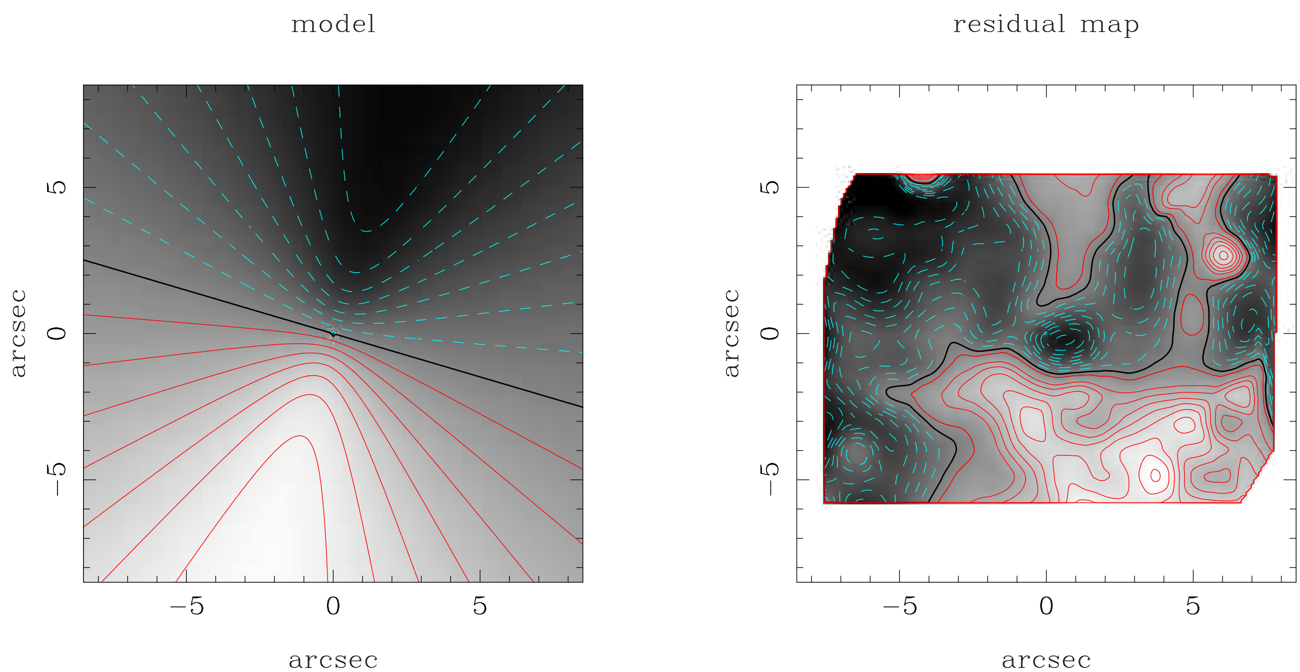

Fig. 17.— a) 2D rotational model built with the stellar velocity curve and projected to the plane of the sky at 42° inclination, the P.A of the line of nodes is 163.5° and the systemic velocity is 2380 km/s. b) Residual velocity map resulting from the subtraction of the disk rotational model from the ionized velocity gas traced by the [NII] emission line. The contours are plotted in steps of 10 km/s. Dashed blue contours go from -80 to -10 km/s, and the full red contours from 10 to 100 km/s.

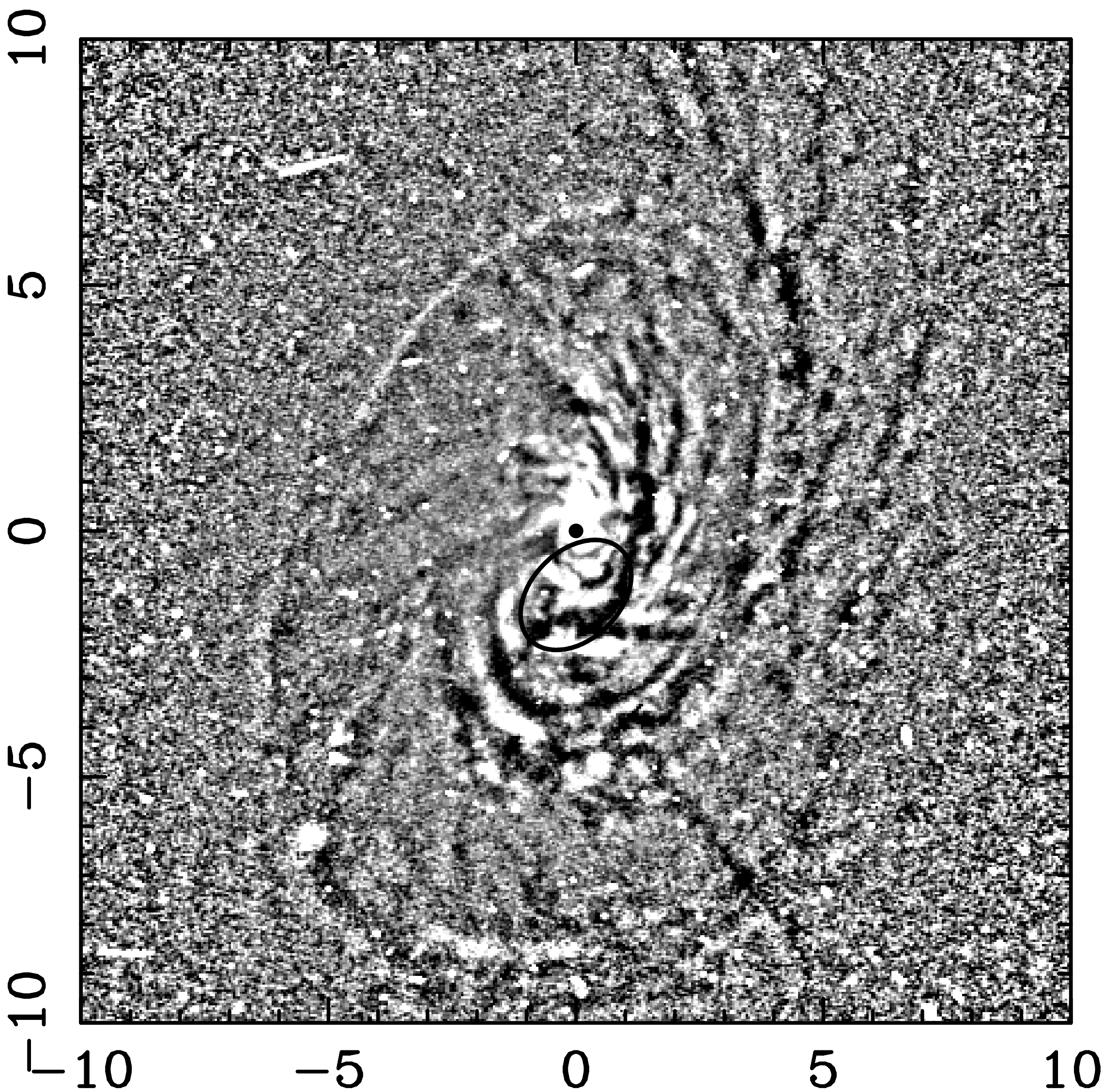

Fig. 18.— Unsharp masked image of NGC 2110 obtained dividing the HST+WFPC2 image through the filter F606W by a median filtered version of the same image (gray scale). The HI absorption cloud detected by Gallimore et al (1999) is plotted as an ellipse.